CellPress
OPEN ACCESS

Trends in
Biotechnology

Research Article

Computationally guided genome rewiring of *Escherichia coli* and its application for nanopolyethylene terephthalate (PET) biodegradation and upcycling

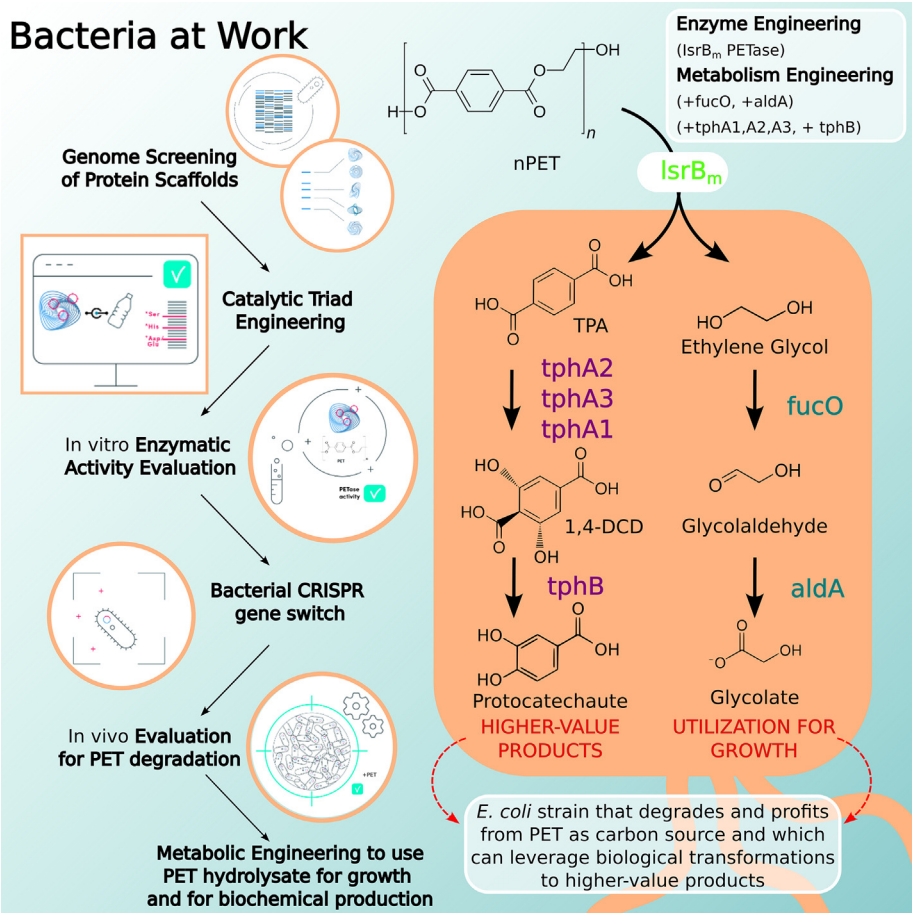

GenRewire is an innovative genome rewiring and editing method that enables *Escherichia coli* to degrade polyethylene terephthalate (PET) nanoparticles without exogenous genetic material. By repurposing native proteins and applying CRISPR/Cas9, this approach advances the field of metabolic engineering for plastic biodegradation and upcycling, while minimizing reliance on foreign gene insertion.

Paula Vidal, Joan Giménez-Dejoz, Laura Fernandez-Lopez, Sonia Romero, Seyed Amirabbas Nazemi, Miguel Luengo, Jose L. Gonzalez-Alfonso, Mireia Martinez-Sugrañes, Ana Robles-Martín, David Almendral, Sergi Roda, Pablo Pérez-García, Luzie Kruse, Karl-Erich Jaeger, Wolfgang R. Streit, Francisco J. Plou, Martin Floor, Patrick Shahgaldian, Rafael Bargiela, Víctor Guallar, Manuel Ferrer

victor.guallar@bsc.es (V. Guallar)
mferrer@icp.csic.es (M. Ferrer).

Highlights

Escherichia coli cannot naturally biodegrade polyethylene terephthalate (PET), because none of its native enzymes are capable of degrading this polymer.

GenRewire, a method that combines computationally guided genome rewiring and CRISPR/Cas9 editing, reprogrammed *E. coli* to degrade PET nanoparticles without introducing foreign DNA.

E. coli protein scaffolds selected for their ability to bind PET were repurposed into variants that degraded PET without compromising their natural function.

Replacement via CRISPR/Cas9 editing enabled *E. coli* to degrade PET nanoparticles, matching the performance of native PET-degrading microorganisms.

Further metabolic engineering enabled safe biomass production and biosynthesis of valuable chemicals from PET.

Trends in Biotechnology, November 2025, Vol. 43, No. 11
https://doi.org/10.1016/j.tibtech.2025.07.008

Trends in Biotechnology

CellPress OPEN ACCESS

Research Article

Computationally guided genome rewiring of *Escherichia coli* and its application for nanopolyethylene terephthalate (PET) biodegradation and upcycling

Paula Vidal [1,10], Joan Giménez-Dejoz [2,10], Laura Fernandez-Lopez [1,10,11], Sonia Romero [2], Seyed Amirabbas Nazemi [3], Miguel Luengo [2,4], Jose L. Gonzalez-Alfonso [1], Mireia Martinez-Sugrañes [2,4], Ana Robles-Martín [2,4], David Almendral [1], Sergi Roda [5], Pablo Pérez-García [6], Luzie Kruse [7], Karl-Erich Jaeger [7,8], Wolfgang R. Streit [6], Francisco J. Plou [1], Martin Floor [2], Patrick Shahgaldian [3], Rafael Bargiela [1], Víctor Guallar [2,9,11,*], and Manuel Ferrer [1,11,*]

Numerous strategies for the biodegradation and upcycling of polyethylene terephthalate (PET) are under investigation. Here, we present a proof-of-concept study for reprogramming the *Escherichia coli* BL21(DE3) strain to degrade PET nanoparticles (nPET) without introducing foreign DNA and compromising native cellular fitness. In brief, native proteins selected *in silico* from the genome were repurposed to acquire artificial PETase activity without compromising their function and were subsequently replaced via CRISPR/Cas9 editing. A variant of the transport protein LsrB, selected for its ability to bind PET, was engineered to degrade PET powder (at 37–60°C). Building on LsrB periplasmic localization, we engineered a strain that degrades nPET at 37°C. The strain was further engineered to grow on nPET degradation products and produce valuable compounds. Our method, which is applicable across diverse genomes and microbial chassis, expands the potential of metabolic engineering to address plastic biodegradation and upcycling while reducing reliance on foreign DNA.

Introduction

Recent years have witnessed rapid scientific and technological advances in sequencing techniques [1], big data meta-analyses [2], artificial intelligence (AI)-driven protein structure prediction [3,4], protein modeling and engineering methods [5,6], and **metabolic engineering** (see Glossary) via **genome-editing technology** [7]. Collectively, these advances have revealed the vast genomic and protein diversity of the biosphere. In addition, they have unlocked novel design strategies for enzymes and cellular biocatalysts that can be harnessed for biotechnological applications.

One such advance is the manipulation of genetic content in model and nondomesticated organisms, enabling the introduction of new functions or the enhancement of existing metabolic functions by integrating new genes encoding desired enzymes or by deleting genes linked to undesirable byproducts or competing pathways. Under optimized fermentation conditions, this genetic manipulation can redirect carbon fluxes to increase the production of targeted

Technology readiness

The development of synthetic biology strategies for polyethylene terephthalate (PET) biodegradation and upcycling continues to present major scientific and engineering challenges. We present GenRewire, a breakthrough strategy for endowing microorganisms with PET-degrading capabilities via genome rewiring and editing without relying on foreign DNA or affecting native fitness. As a proof of concept, we engineered *Escherichia coli* BL21 (DE3) to degrade PET nanoparticles and further convert the polymer to safe biomass and valuable chemicals. This method integrates deep learning-driven protein engineering and CRISPR-based editing to repurpose native proteins by endowing them with artificial PET-degrading activity and stably integrating this new function into the genome without compromising metabolic integrity. GenRewire presents an advantage over traditional metabolic engineering approaches, because it enables the incorporation of PET biodegradation capacity by reprogramming endogenous proteins rather than relying on the integration of foreign DNA typically required to express heterologous PETases. By combining artificial intelligence (AI)-driven protein structural prediction with advanced molecular modeling tools [e.g., Protein Energy Landscape Exploration (PELE) Monte Carlo], this strategy enables the rational design of PET-degrading *E. coli* strains

compounds. For example, Fu and colleagues successfully reprogrammed *Yarrowia lipolytica* for efficient itaconic acid production [8]. In addition, a broad array of **synthetic biology** strategies, including plasmid delivery or gene editing, enables the introduction in a host cell of new metabolic pathways, thereby creating cell factories capable of tailored biosynthesis. Li and colleagues demonstrated this by integrating a β-carotene synthesis pathway into *Escherichia coli*, achieving β-carotene production through fed-batch fermentation [9].

Current reprogramming methods for engineered microbes face challenges, such as a negative impact on cellular metabolism, when specific genes are interrupted. Furthermore, the instability of replicating plasmids often necessitates pathway reoptimization upon chromosomal integration [8]. Metabolic engineering also depends on the integration and expression of foreign genes, which remains challenging. Techniques, such as transposon- and homologous recombination-based technologies, can integrate heterologous DNA into the genome, but can cause inconsistent host–pathway interactions owing to unpredictable integration sites. Replacing native promoters with stronger or weaker promoters from other species can address some problems, such as the regulation of nitrogen limitation or the modulation of gene copy number for selected target combinations [8]; however, the versatility of these approaches is limited and varies between species. These limitations could be overcome by reprogramming the activities of proteins encoded within a given genome via structure-guided engineering, ensuring that the proteins retain their original functions while acquiring novel enzymatic activities. This approach eliminates the need to introduce foreign DNA while streamlining time-consuming and costly processes of metabolic disruption, carbon flux redirection, and regulatory system modification traditionally associated with strain engineering to ensure increased growth rates and product yields [8].

Protein engineering has been revolutionized by recent developments in computer simulations and AI-based algorithms, which, for example, allow the generation of *de novo* enzyme scaffolds [10] and optimization of their sequences for increased stability [11–13]. Moreover, *de novo* enzyme designs using deep learning techniques can produce enzymes that approach native catalytic rates [14,15]. These designs are typically built around constrained active sites, enforcing catalytic geometries. By contrast, researchers have pioneered the **PluriZyme** concept, a different approach that introduces artificial hydrolytic active sites by transforming substrate binding sites into catalytic sites [5,6,16,17]. This approach ensures better substrate diffusion and binding while introducing only a few point mutations to assemble, for example, a Ser–His–Asp catalytic triad that supports ester hydrolysis; it can also combine different biochemistries in a single enzymatic scaffold, allowing one-enzyme cascade reactions [18], a feature further enhanced by the introduction of metal-complex chemocatalytic sites [5].

The PluriZyme concept, particularly its recent application to confer PET-degrading activity to a selected protein scaffold, such as a pore-forming protein [6], inspired the transformation of a model bacterial strain, namely, *E. coli* BL21 (DE3), into a PET degrader. This enabled the strain to exploit this environmentally harmful polymer for safe biomass production and further bioconversion. This goal was achieved by developing a novel methodological approach, hereafter referred to as GenRewire, to extend the design of artificial catalytic sites to the genome scale. We conducted a thorough analysis of the *E. coli* BL21 (DE3) genome and strategically incorporated artificial PET hydrolase catalytic sites into protein scaffolds selected based on specific criteria. Importantly, these native scaffolds do not have any inherent ability to degrade PET in any of its forms, including films, powders, or particles of various sizes. The genes encoding the repurposed enzyme variants are then reintroduced into the genome via genome editing to replace the original proteins. Metabolic engineering further equips the microorganism

in just 2–3 months, with potential applicability to other microbial chassis. With these advances, our strategy has reached technology readiness level (TRL) 4 in NASA's Technology Readiness Level system. Moreover, GenRewire is more than a simple alternative and can serve as a complementary tool to traditional metabolic engineering, as demonstrated in this work for PET nanoparticle upcycling.

[1]Instituto de Catalisis y Petroleoquimica (ICP), CSIC, 28049 Madrid, Spain
[2]Barcelona Supercomputing Center (BSC), 08034 Barcelona, Spain
[3]School of Life Science, University of Applied Sciences and Arts Northwestern Switzerland, CH-4132 Muttenz, Switzerland
[4]PhD Program in Biotechnology, Faculty of Pharmacy and Food Sciences, University of Barcelona, 08028 Barcelona, Spain
[5]Nostrum Biodiscovery, 08029 Barcelona, Spain
[6]Department of Microbiology and Biotechnology, University of Hamburg, 22609 Hamburg, Germany
[7]Institute of Molecular Enzyme Technology, Heinrich Heine University Düsseldorf, 52426 Jülich, Germany
[8]Institute of Bio- and Geosciences IBG-1: Biotechnology, Forschungszentrum Jülich GmbH, 52426 Jülich, Germany
[9]Institució Catalana de Recerca i Estudis Avançats (ICREA), 08010 Barcelona, Spain
[10]These authors are joint first authors
[11]These authors contributed equally to this work

*Correspondence:
victor.guallar@bsc.es (V. Guallar) and
mferrer@icp.csic.es (M. Ferrer).

with the ability to utilize PET degradation products, such as ethylene glycol (E) for growth and terephthalic acid (T) for the biosynthesis of valuable compounds, specifically protocatechuate (PCA).

In this work, our goal was to neither create PET hydrolases that surpass previously engineered ones nor engineer an *E. coli* strain that outperforms previously published strains for PET biodegradation and upcycling. Instead, this proof-of-concept work aimed to implement and assess the suitability of a novel strategy for building artificial PET-hydrolyzing enzymes on intrinsic *E. coli* scaffolds. Our approach enables the engineering of an *E. coli* strain capable of degrading nPET without relying on externally supplied PETases. More generally, our results suggest the potential of GenRewire to repurpose native proteins within the genome of a cellular system while minimizing the reliance on foreign DNA.

Results

Computational and experimental workflow for genome rewiring

GenRewire comprises several computational and experimental steps (Figure 1). The first step is an analysis of the bacterial genome to select protein targets. In step 2, we computationally generate the 3D structures of all the selected proteins, a task that is only possible because of the development of deep learning structural predictors. Massive **protein energy landscape exploration (PELE)** of model substrates is carried out with all selected proteins to identify putative binding pockets (step 3) and to insert the catalytic triads (step 4), generating a final list of protein candidates. In step 5, *in vitro* experiments validate the proteins selected *in silico*, defining the mutations that will be inserted by **CRISPR** editing (step 6). The final step involves *in vivo* evaluation of the engineered bacteria. The entire procedure and its implementation are described later.

For steps 1–4, although a detailed discussion is provided later, protein scaffolds were selected based on specific criteria, including: (i) a size range of 100–450 amino acids, the presence of signal peptides or transmembrane domains, and the ability to generate 3D structures with high confidence [predicted Local Distance Difference Test (pLDDT) score >70]; (ii) the presence of binding pockets located at least 6 Å away from native catalytic residues, and exhibiting favorable binding energies for the target substrates (ETETETE: <–39.95 kcal/mol; ETETE: <–32.06 kcal/mol; MHET: <–24.67 kcal/mol); and (iii) the capacity, following the incorporation of artificial Ser–His–Asp catalytic triads, to maintain catalytically competent geometries (interatomic distances <3.5 Å), with the triad remaining in a catalytically active conformation for >35% of the simulation time.

Genome analysis and binding site selection for catalytic triad protein engineering

As a model strain, we chose the *E. coli* strain BL21 (DE3), a widely used host in research and industry, and used the protein-coding genes annotated in the UniProt database (accession code UP000000625; https://www.uniprot.org/proteomes/UP000000625). We retained proteins between 100 and 450-amino acids long, excluding proteins lacking signal peptides and transmembrane proteins, with the aid of SignalP5.0 [19] and DeepTMHMM [20]. We obtained 386 presumptive extracellular or periplasmic soluble proteins to scan for potential binding sites. This filter was applied because, as a proof of concept, we aimed to generate a bacterium capable of degrading nPET. This required the proteins to be either extracellular or membrane anchored; however, this filter may not be necessary for other applications. We retrieved the structures of these proteins from the Protein Data Bank (PDB) [21,22] or the AlphaFold protein structure database [3,23] or by running AlphaFold 2.0 [3], removing models with low confidence scores.

Glossary

CRISPR: precise, efficient gene-editing method derived from the bacterial immune system (CRISPR/Cas9), enabling targeted DNA modifications via guide RNAs and Cas nucleases. These modifications are based on the generation of site-specific double-strand breaks in the DNA, which are then repaired by the cell via nonhomologous end joining (NHEJ) or homology-directed repair (HDR), leading to insertions, deletions, or precise sequence replacements.

Genome-editing technology: tools and methods, including CRISPR, that enable accurate insertion, deletion, or replacement of DNA sequences within genomes. These technologies can be applied to almost any genome, from microorganisms to plants and animals, and allow for single or multiple edits, including point mutations, gene knockouts, or large-scale insertions and rearrangements. Genome editing facilitates precise manipulation of genetic information for research, therapeutic, agricultural, and industrial purposes.

Metabolic engineering: modification of cellular metabolic pathways through genetic or regulatory changes to enhance or redirect the production of specific molecules. This process often involves the introduction of heterologous DNA to confer new biosynthetic capabilities. Subsequent optimization typically requires targeted modifications to the host genome to fine-tune native regulatory networks and improve flux toward the desired metabolic outcome.

PluriZyme: computationally designed enzyme that incorporates multiple active sites within a single protein scaffold, enabling it to catalyze more than one chemical transformation independently or in tandem. To introduce artificial active sites, potential binding pockets are first identified based on favorable binding energies for the target substrates. These pockets are then converted into catalytic sites by introducing catalytic residues that adopt and maintain catalytically competent geometries, ensuring that the residues remain in a catalytically active conformation.

Protein energy landscape exploration (PELE): Monte Carlo computational method that maps the energy landscape of intermolecular interactions, being highly specialized in protein–ligand interactions. In this work,

Using the PluriZyme protocol, we first scanned the protein surfaces of all candidates via the Global Exploration (GE) module of PELE software to identify substrate-binding sites [5,6,17] (Figure 2A). We used as substrate models three soluble products that are part of PET, a high-molecular-weight polymer [24], namely: ETETETE, ETETE, and TE. In this nomenclature by Schubert and colleagues [24], T and E are linked by ester bonds in a PET chain. We selected the top 100 proteins for each substrate according to their binding energy to the surfaces of the proteins. Specifically, we searched for proteins that accommodate multiple substrates at a single binding site. This comparison allowed us to select 42 proteins with this ability: 22 that bound both ETETETE and ETETE, nine that bound both ETETE and TE, eight that bound both ETETE and TE, and three that bound all three substrates. These proteins exhibited binding interactions at consistent locations, indicating their potential versatility in substrate binding. We selected 25 protein candidates for design, excluding locations near native enzyme active sites (within 6 Å of known catalytic residues) to prevent interference with wild-type activity. In this way, we engineered natural protein variants that did not interfere with bacterial metabolism, as clearly demonstrated by the fitness experiments (see later).

PELE is used to first scan the protein surfaces of all candidate proteins using the Global Exploration (GE) module of the PELE software to identify potential binding sites for the target substrates.
Synthetic biology: interdisciplinary field that applies engineering principles, such as iterative design–build–test–learn cycles, to biology, enabling the construction of novel biological systems and the redesign of existing organisms. It relies on standardized genetic parts (e.g., promoters, ribosome binding sites, coding sequences, terminators, and regulatory elements) that can be assembled into functional modules or circuits. Synthetic biology can be applied to a range of biological systems, including prokaryotes and eukaryotes, with applications spanning biomedicine, biotechnology, environmental remediation, and more.

Second, we systematically designed Ser–His–Asp catalytic triads (see STAR★METHODS), resulting in 673 protein variants that were ranked via protein–substrate PELE-induced fit simulations (Figure 2B,C). Prioritization was based on the interaction energy and fulfillment of catalytic distance metrics (Figure 2B), defining a free energy catalytic matrix (FECM; see STAR★METHODS) that was compared with those from reference PETase simulations. In total, 88 triads were selected for the last refinement step via all-atom molecular dynamics (MD) simulations to check the stability of the substrate and triad in the binding site (Figure 2D). Twenty-three variants from 18 proteins were ultimately chosen for experimental validation. The sequences and expression systems used in this study are detailed in Data S1A–C in the supplemental information online.

In vitro evaluation of PETase activity in engineered *E. coli* proteins

The native and mutant genes were synthesized, and the activity of the purified proteins (Figures S1 and S2 in the supplemental information online) was evaluated with ETE [or bis(2-hydroxyethyl) terephthalate, BHET], a model substrate structurally analogous to those used in the MD simulations. Among the synthetic variants, $YggN_m$ (engineered by introducing the A91S and M131H mutations into the outer membrane protein YggN) exhibited only low activity against ETE (specific activity: 0.48 μmol/min/g at 37°C and pH 7.0), as determined by high-performance liquid chromatography (HPLC) analysis. By contrast, $SsuA_m$ (A65S, P67H, and P87D) and $LsrB_m$ (G318S, D317H, and S287D) displayed significantly higher activities, with specific activities of 368 and 503 μmol/min/g, respectively (Data S1D and Table S1 in the supplemental information online).

Given that ETE is a soluble PET fragment commonly used as a screening substrate to indicate potential PETase activity, we evaluated the ability of the three variants to cleave PET powder (maximum particle size: 300 μm; hereafter referred to as pPET) using HPLC measurements (see STAR★METHODS). Four temperatures (37, 40, 50, and 60°C) were selected, including 37°C, because the engineered enzymes are expected to function at the optimal growth temperature of *E. coli*, the host organism used in our proof-of-concept study. Demonstrating activity at 60°C would not indicate function in *E. coli.* For comparison, we evaluated the activity of the purified (Figure S3 in the supplemental information online) specialized, optimized benchmark PETase variants, LCC-ICCG [25] and HotPETase [26], under the same conditions, at 37°C. Assessment of their performance at elevated temperatures was not performed because such data have been reported previously [27].

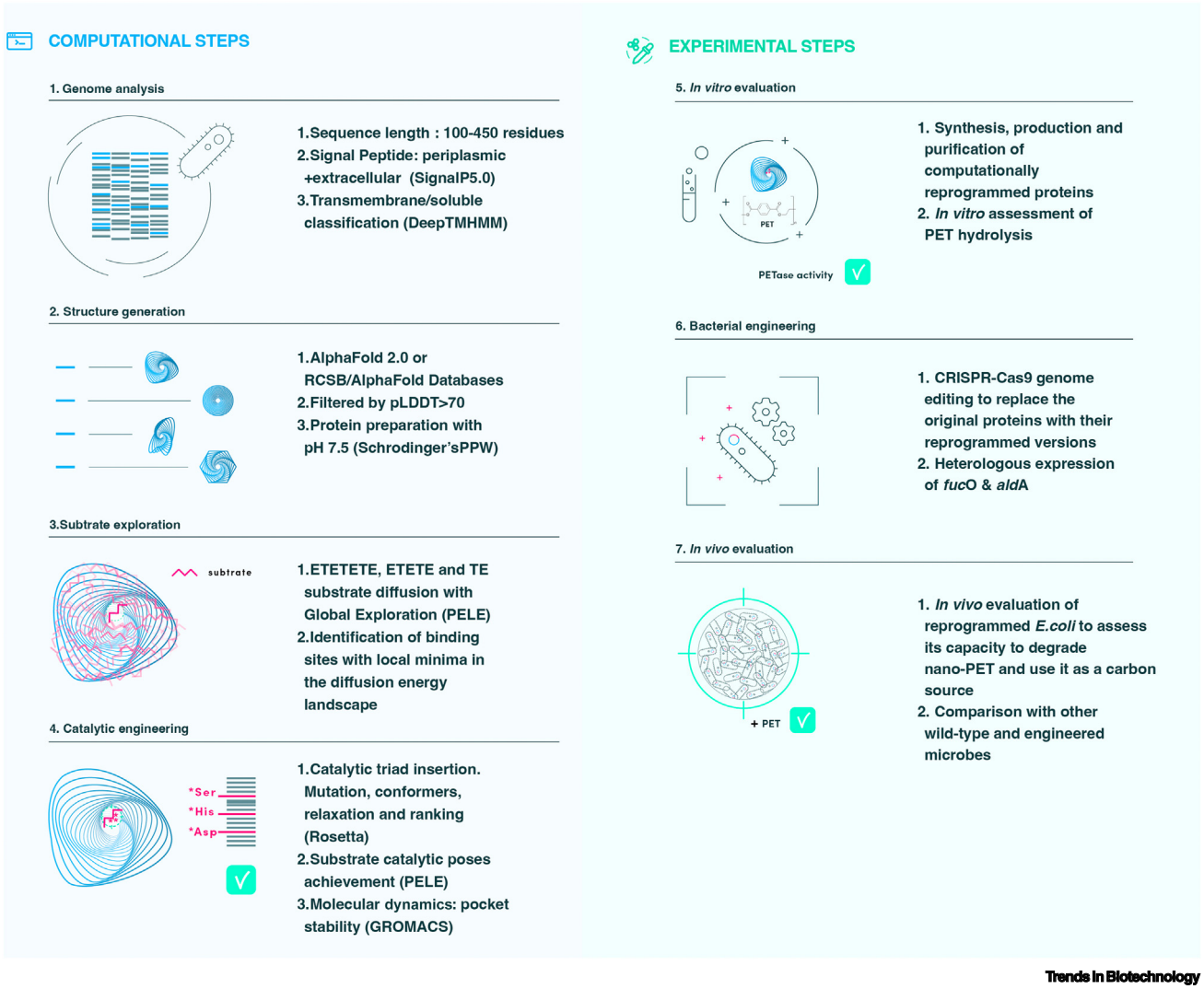

Figure 1. GenRewire pipeline. Schematic depicting the computational and experimental steps of our novel approach to confer PET nanoparticle biodegradation capacity to a bacterial strain. Step 1: bacterial genome analysis. Step 2: generation of 3D protein structures. Step 3: identification of potential substrate binding pockets. Step 4: insertion of the catalytic site (Ser–His–Asp triads in this study) and ranking of the designs. Step 5: validation experiments *in vitro*. Step 6: editing the bacterial genome via CRISPR/Cas9. Step 7: *in vivo* evaluation of the engineered bacteria. The different software used in the computational steps are in parentheses. Abbreviations: PELE, protein energy landscape exploration; pLDDT, predicted Local Distance Difference Test.

Under the specific conditions used in this study, which differ from those that are relevant for large-scale hydrolysis [27], degradation tests revealed that, at 37°C and pH 7.0, only $SsuA_m$ (0.22 μmol degradation products/h/mg enzyme) and $LsrB_m$ (0.86 μmol/h/mg enzyme) were able to degrade PET powder, whereas $YggN_m$ displayed no detectable activity (Table 1 and Data S1E in the supplemental information online). At this temperature and pH, LCC-ICCG and HotPETase exhibited relatively high degradation rates, namely 1.90 and 1.75 μmol/h/mg enzyme, respectively. Both engineered enzymes, $SsuA_m$ and $LsrB_m$, showed activity on PET powder across a wide temperature range, reaching degradation rates of up to 2.74 ($SsuA_m$) and 19.62 ($LsrB_m$) μmol/h/mg enzyme at 60°C; at this temperature, no degradation was observed with the $YggN_m$ variant. Although significant, these values are lower than those reported for benchmark PETases under

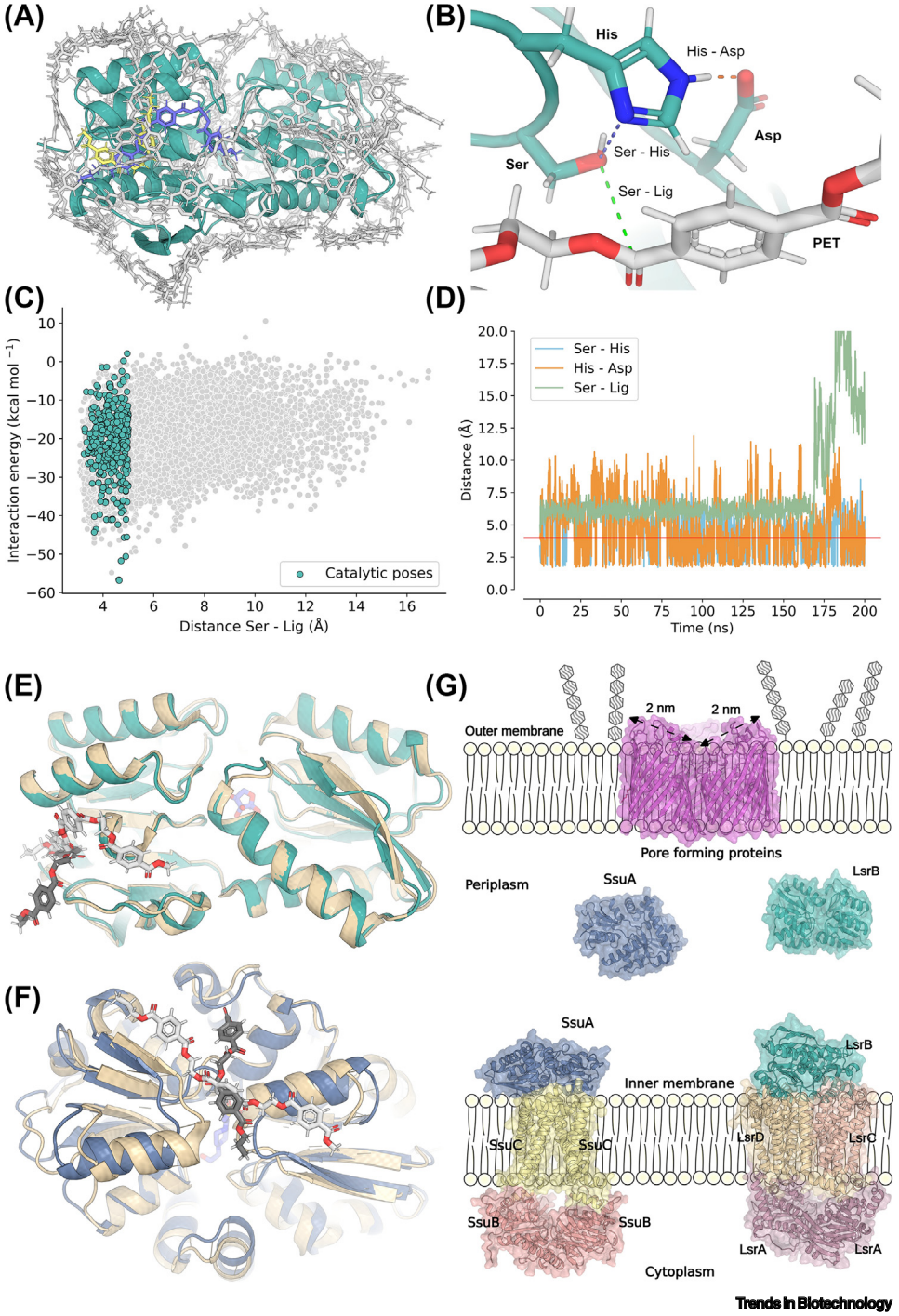

Figure 2. Artificial PET-ase active sites designed in two native *Escherichia coli* scaffolds. The Protein Energy Landscape Exploration (PELE) and molecular dynamics (MD) simulation results, catalytic triad configurations, structural models, and subcellular localizations of the engineered proteins are shown. (A) PELE Global Exploration (GE) of LsrB (UniProt accession number: A0A140NCA9) with ETETETE (gray sticks, where E is ethylene glycol and T is terephthalic acid). The image illustrates exhaustive surface sampling, with the best-ranked positions corresponding to lower interaction energies highlighted in blue. For comparison, the best-ranked positions of ETETE are also shown (in yellow). (B) Catalytic residues (serine, histidine, and aspartic acid) inserted into LsrB following a PELE-induced fit simulation. The resulting complex with the PET substrate is shown as a

(Figure legend continued at the bottom of the next page.)

thermal and pH conditions relevant for large-scale hydrolysis [27] (Table S2 in the supplemental information online).

After confirming the activity against PET powder, we next evaluated the ability of the $SsuA_m$ and $LsrB_m$ variants to degrade PET particles with sizes between 1 and 5.5 nm (hereafter referred to as nPET). These particles were prepared because they can cross the pores in the outer membrane of *E. coli* within 1–3 h [28] and, if degraded by any of the variants at 37°C, these nanoparticles could be used in subsequent *in vivo* assays within the framework of our proof-of-concept work. Therefore, degradation assays using synthetic nPET (see STAR★METHODS) from Goodfellow's amorphous PET film were conducted at 37°C and pH 7.0. Under the specific conditions used, $SsuA_m$ and $LsrB_m$ released 2.16 and 5.15 μmol/h/mg enzyme, respectively (Table 1 and Data S1E), values slightly lower than those of the benchmark enzymes LCC-ICCG (12.60 μmol/h/mg enzyme) and HotPETase (10.36 μmol/h/mg enzyme), which were tested under the same conditions.

Using electrospray ionization–mass spectrometry (ESI–MS) (Figure S4 and Data S2A in the supplemental information online), we confirmed that the degradation products identified by HPLC included TET, ETE, TE, and T (Data S1E) when both $SsuA_m$ and $LsrB_m$ were used. Using nPET as a model substrate, we further evaluated the temperature and pH profiles of both proteins, finding maximum activity at 60–70°C (Data S1E and Figure S5A in the supplemental information online) and pH 7–8 (Figure S5B and Data S1E).

This confirmed that we had introduced *de novo* PET hydrolysis ability into two *E. coli* proteins, neither of which naturally degrades PET in either powder or nanoparticle form. One of them is the autoinducer 2 (AI-2)-binding protein LsrB (UniProt A0A140NCA9), a periplasmic protein that is part of the ABC transporter complex LsrABCD and is involved in AI-2 import [29]. The protein has a hinge linking two similar α/β domains where the binding site is located [30], far from the position where ETETETE and ETETE can be accommodated (Figure 2E). The other is SsuA (UniProt A0A140ND91), a periplasmic aliphatic sulfonate-binding protein involved in the assimilation of sulfur from organic compounds, such as sulfate esters, sulfamates, sulfonates, and alkanesulfonates [31], which is crucial for the biosynthesis of the sulfur-containing amino acids L-methionine and L-cysteine. SsuA is a monomeric protein comprising two domains (I and II), and both ETETETE and ETETE substrates are bound to domain I, which is far from the putative active site [31] (PDB 3e4r) (Figure 2F). In summary, both proteins are located on the outer side of

basis for assessing the catalytic metrics. (C) Energy profile of the PELE-induced fit simulation for LsrB with ETETE. Poses that fulfill the catalytic metrics (in terms of Ser–Lig distance, where Lig refers to the ETETE ligand) are in green. (D) Distance between the catalytic residues and the PET substrate ETETE through the MD simulation for LsrB. The 4-Å threshold used to filter the MD results is in red. (E) $LsrB_m$ structure with substrates bound at both the native and engineered binding sites. The $LsrB_m$ structure (green cartoon), which resembles the LsrB structure from *Yersinia pestis* (PDB: 3t95, yellow cartoon), displays two α/β domains connected by a hinge. It is shown with an autoinducer 2 (AI-2) molecule bound in the native active site (blue sticks) and ETETETE (light gray) and ETETE (dark gray) bound in the engineered binding site. (F) $SsuA_m$ structure with substrates bound at both the native and engineered binding sites. The $SsuA_m$ structure (blue cartoon) is compared with the SsuA structure from *E. coli* [Protein Data Bank (PDB): 3e4r, yellow cartoon), which contains a bound substrate [4-(2-hydroxyethyl)-1-piperazineethanesulfonic acid (HEPES); blue sticks], with ETETETE (light gray) and ETETE (dark gray) shown in the engineered binding site. (G) Schematic of the locations of LsrB and SsuA within the *E. coli* cell envelope. Both proteins are part of the LsrABCD and SsuABC transporters. The full transporter complexes are shown, along with free, unbound forms of LsrB and SsuA. To generate protein transporter images of LsrA, LsrC, and LsrD, structure models were obtained from the AlphaFold database (AF-P77257-F1-v4, AF-P77672-F1-v4, and AF-P0AFS1-F1-v4, respectively), along with models of SsuC and SsuD (AF-P75851-F1-v4 and AF-P0AAI1-F1-v4, respectively). The porin structure of OmpF, depicted in the outer membrane, was obtained from PDB entry 2ZFG. (A–D) Created with PyMOL (Version 2.5 Schrödinger, LLC), and graphs created with the Python Matplotlib and Seaborn libraries (see STAR★METHODS).

Table 1. Specific activity measured during the hydrolysis of pPET and nPET at different temperatures by engineered $SsuA_m$ and $LsrB_m$, compared with optimized benchmark PETase variants HotPETase and LCC-ICCG

Substrate[a]	Temperature (°C)	Specific activity (μmol/h/mg enzyme)[b]			
		$SsuA_m$	$LsrB_m$	HotPETase	LCC-ICCG
pPET	37	0.22 ± 0.00	0.86 ± 0.10	1.75 ± 0.17	1.90 ± 0.08
	40	0.34 ± 0.04	1.09 ± 0.10	n.d.	n.d.
	50	1.36 ± 0.11	7.63 ± 0.03[c]	n.d.	n.d.
	60	2.74 ± 0.11[c]	19.62 ± 0.59[c]	n.d.	n.d.
nPET	37	2.16 ± 0.04	5.15 ± 0.09	10.36 ± 0.99	12.60 ± 1.15

[a]Reaction conditions: [pPET], 7 mg/ml or [nPET], 1.65 mg/ml; [enzyme], 0.1 mg/ml; buffer, 50 μl of 40 mM HEPES buffer; pH, 7.0; agitation, 950 rpm. The reaction times were set to 0, 2, 4 and 24 h. Analyses were performed by HPLC. All values represent the means of three independent biological replicates (n = 3), with standard deviations calculated using the STDEV.S function in Excel 2019. Unprocessed data are available in Data S1E in the supplemental information online.
[b]For quality control, two variants with nonproductive active sites were synthesized without informing the group responsible for producing, purifying, and characterizing the enzymes. Once the assays were completed, the results for all the variants, including the nonproductive ones, were sent to the team responsible for computational analysis and design of the mutations. Cross-checking confirmed that none of the nonproductive variants were active, reinforcing the validity of the method through blind tests.
[c]Only 2-h data were used for calculations.

the inner membrane [29–31], which is exposed to the periplasm (Figure 2G), a space accessible by ultrasmall nanoparticles (<5 nm) [28].

Engineering genome-rewired *E. coli* to use PET hydrolysates as a carbon source

We replaced *lsr*B_{WT} with *lsr*B_m in the *E. coli* BL21 (DE3) genome via CRISPR/Cas9 with the aim of obtaining a genome-rewired *E. coli* strain capable of depolymerizing nPET with a size <5 nm. We selected the protein LsrB because its variant, $LsrB_m$, exhibited greater activity in our assays toward nPET and pPET compared with the variant of SsuA, $SsuA_m$ (Table 1 and Data S1E). In addition, *fucO* (acc. nr. AAB40449.1) and *aldA* (acc. nr. WP_000115943.1) from *E. coli* MG1655, which support the metabolism of E [32,33], were heterologously incorporated [using the pET-45b(+) vector]. FucO and AldA channel E into the central metabolism for growth via glycerate metabolism [33]. Thus, two *E. coli* BL21 (DE3) strains were generated: one with *fuc*O and *ald*A in the genome-rewired strain (with *lsr*B_{WT} replaced with *lsr*B_m) and the other with *fuc*O and *ald*A in the original strain (with *lsr*B_{WT}). We refer to these strains as strains S1 and S2, respectively. The FucO and AldA expression levels in both strains were satisfactory and comparable (Figure S6 in the supplemental information online).

We first evaluated the fitness and E utilization of engineered strain S1 compared with those of strain S2 by measuring their growth rates. Since the impact of these edits may depend on growth conditions [34], we grew triplicate cultures of the S1 and S2 strains in Luria–Bertani (LB) medium, minimal M9 medium supplemented with 10 mg/ml glucose, and M9 medium supplemented with 10 mg/ml E and 0.10 mg/ml glycerol, which was found to increase E utilization [32]. Cultivations were performed for 24 h at 37°C in a 96-well plate with constant shaking. The growth rate of the genome-rewired strain (S1), measured during the exponential growth phase, was not significantly different from that of the parental strain (S2) under any of the three conditions (Figure 3A–D; Data S1F and Table S3 in the supplemental information online). The selection coefficients (S) further revealed changes in fitness of <5% (Table S3), indicating that genome rewiring had no significant effect on fitness. Once we confirmed that there was no significant effect on fitness and that strain S1 was capable of using E as a carbon source, we proceeded to evaluate whether strain S1 could use nPET particles as a carbon source.

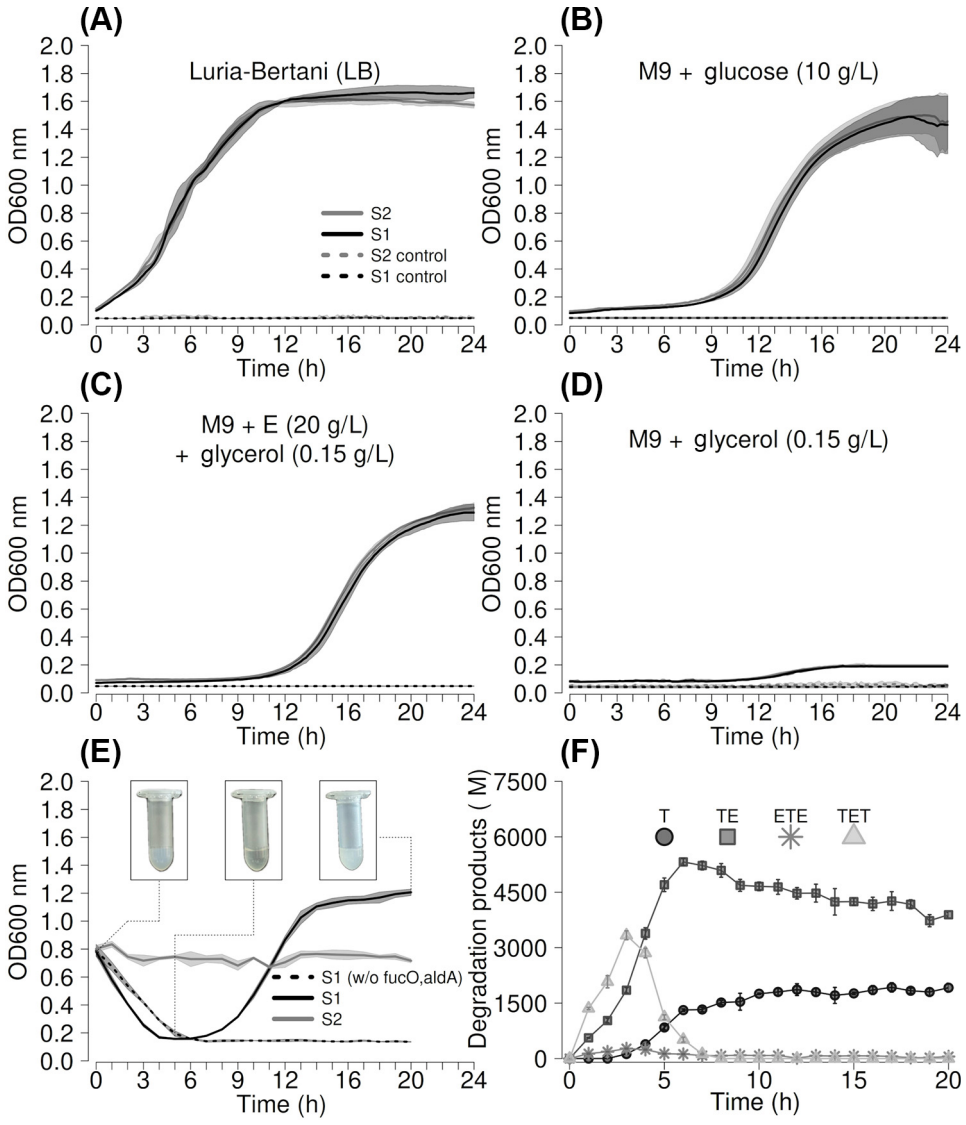

Figure 3. Fitness evaluation and *in vivo* degradation of PET nanoparticles (nPET) by genome-rewired strains. (A–E) Bacterial growth monitored by optical density (OD_{600nm} measurements over time of strains S1 and S2 across various growth media: (A) Luria–Bertani (LB) medium; (B) M9 with glucose (10 mg/ml); (C) M9 with ethylene glycol (E) (20 mg/ml) and glycerol (0.10 mg/ml); (D) M9 with glycerol (0.10 mg/ml); (E) M9 medium with glycerol (0.10 mg/ml) and nPET (1.3 mg/ml). (E) displays three representative images depicting the whitish suspension of nPET particles at time 0, the transition of the suspension to transparency at 5 h, and subsequent cellular growth resulting in a turbid suspension again (see Video S1 in the supplemental information online). The cultivation conditions were as follows: medium supplemented with 100 μg/ml ampicillin (Amp) and 1 mM IPTG; initial OD_{600nm} of 0.1; 37°C; and incubation for 20 h (for details, see STAR★METHODS). (F) Degradation products quantified by HPLC during *in vivo* culture of strain S1, as shown in (E). In all cases, the values (unprocessed data available in Data S1F in the supplemental information online) are the means of three biological replicates (n = 3), with standard deviations calculated using the STDEV. S function in Excel 2019. The data for S1 are in black, whereas those for S2 are in gray. The corresponding control samples are represented by broken lines. The area around the lines represents the standard deviation between the triplicate data taken at each timepoint. Figure created using the R programming language v.4.4.1, with core-base functions and in-house scripts. Abbreviation: T, terephthalic acid.

The nPET particles from Goodfellow's PET amorphous film were prepared as detailed in the STAR★METHODS. The size was confirmed via atomic force microscopy (AFM; Figure 4). The micrographs revealed that the particles aggregated in two dimensions, mainly as monolayers and multilayers (aggregates). Roughness analysis of the gold-coated particles (Figure 4A) revealed two prominent distribution peaks, one at 1.0 nm and the other at 5.5 nm, corresponding to the roughness of the substrate (silicon wafer, which can be neglected) and a film comprising small spherical nPET particles (confirmed by scanning electron microscopy; SEM), respectively (Figure 4B). This result was confirmed by line profile analyses (Figure 4C). Lines drawn (numbered 1–3 in Figure 4A) over both the substrate (dark brown) and the monolayer sample area (brown) revealed consistent heights of ~1 nm and 5.5 nm, respectively. The formation of PET films and aggregates from small PET particles was confirmed by SEM (Figure 4D). This alignment between roughness and line profile analyses indicates that the average height and, thus, the size, of the nPET is 4.5 nm.

The S1 strain was cultured in M9 medium supplemented with nPET particles (1.3 mg/ml final concentration) at 37°C. During cultivation, we observed a decrease in optical density (Figure 3E and Data S1F in the supplemental information online), indicating active degradation of the particles, as

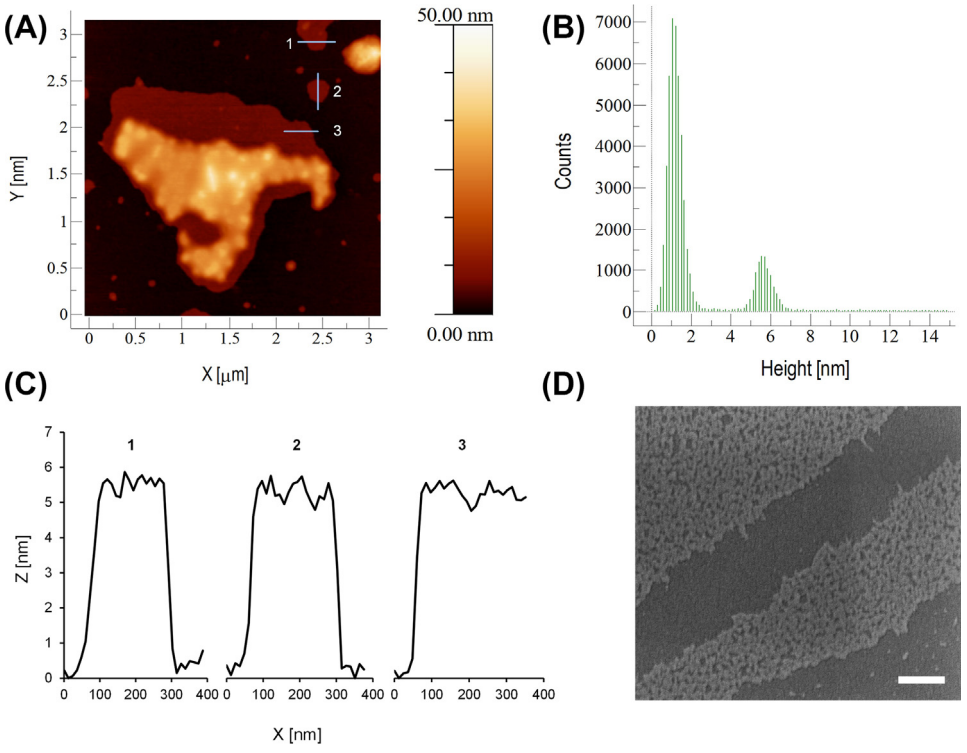

Figure 4. Atomic force microscopy (AFM) and scanning electron microscopy (SEM) analysis of PET nanoparticles (nPET). (A) AFM micrograph of nPET mono- and multilayer films spread over a silicon wafer substrate. (B) Roughness analysis of the entire AFM micrograph presented in (A) revealing two major height distribution peaks at 1 and 5.5 nm corresponding to the roughness of the substrate and nPET particles organized as monolayer films, respectively. (C), Line profile analysis of the AFM micrograph over the drawn lines numbered 1–3 in (A), indicating the constant height of the nPET monolayer at 5.5 nm. (D) SEM micrograph of nPET particles illustrating the distribution and aggregation of single nPET particles, leading to the formation of a monolayer. Scale bar: 200 nm. At least 100 measurements were performed for each sample. The gold coating could influence the particle diameter; thus, the actual size of the particles could be relatively small.

confirmed by HPLC analysis. Indeed, after 6 h, the cloudy suspension of nPET became transparent (Figure 3E, Data S1F, and Video S1 in the supplemental information online), at which point this strain efficiently produced 7263 ± 215 μM degradation products (Figure 3F and Data S1F). Initially, the primary degradation product was TET, which was further degraded to TE and T as the main products.

We further observed that the S1 cells used the E present in the hydrolysate as a carbon source through the action of FucO and AldA, thereby promoting growth (Figure 3E, Video S1, and Data S1F). For our engineered strain, we observed a maximum growth rate of ~0.328 ± 0.02 h^{-1} between 8 and 12 h, corresponding to a doubling time of ~2.1 ± 0.1 h, with a final optical density $(OD)_{600\ nm}$ of ~1.328 ± 0.02 after 20 h (Figure 3E and Data S1F). When we used the S1 strain without *fuc*O and *ald*A, degradation was observed, but no appreciable growth was detected (Figure 3E and Data S1F) because of the lack of genes required for E metabolism. Under the same conditions, strain S2 showed no appreciable growth or degradation (Figure 3E and Data S1F).

Comparative nPET degradation by genome-rewired *E. coli* and native strains

Comparison of the efficiency of our genome-rewired *E. coli* strain in degrading nPET to that of other strains, either native or engineered through various strategies, is challenging. First, most studies use PET films or powders as substrates (Table S4 in the supplemental information online) rather than nPET, which exhibit distinct physicochemical and structural properties. Second, a fair comparison would require an *E. coli* strain expressing a heterologous PETase, preferably of mesophilic origin, given that all the assays were conducted at 37°C. In addition, the enzyme should be secreted into the periplasmic space (as for $LsrB_m$) or extracellularly to ensure effective access to the nanoparticles.

To address the limited data available in the literature for such a comparison, we selected five bacterial strains, *Stutzerimonas stutzeri*, *Halopseudomonas litoralis*, *Halopseudomonas oceani*, *Halopseudomonas aestusnigri*, and *Halopseudomonas bauzanensis*, which produce extracellular PETase-like enzymes, as evidenced by halo formation on agar plates containing Impranil® DLN [35]. The strains were cultured with nPET at mesophilic temperature (28°C; optimal growth temperature) under the same conditions as strain S1. After 24 h, the degradation products were analyzed by HPLC. Their concentrations ranged from 18 to 94 μM, with T or T+ETE as the main product depending on the strain (Figure 5 and Data S1G in the supplemental information online).

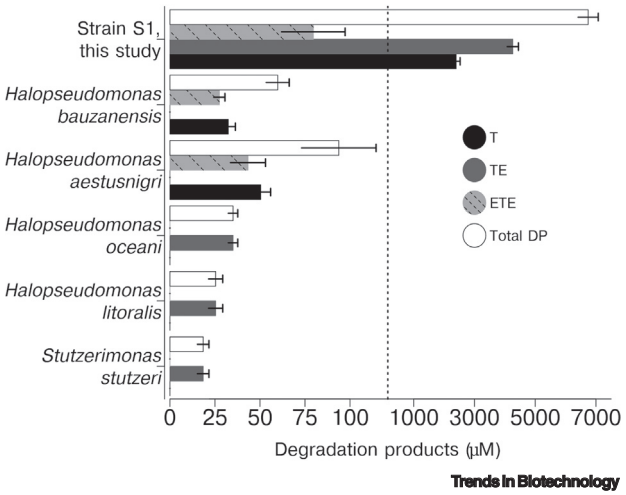

Figure 5. *In vivo* degradation of polyethylene terephthalate nanoparticles (nPET) by native strains. Degradation products (DPs) of *Stutzerimonas stutzeri, Halopseudomonas litoralis, Halopseudomonas oceani, Halopseudomonas aestusnigri, and Halopseudomonas bauzanensis* quantified by HPLC (Data S1G in the supplemental information online) during *in vivo* culture at 28°C and 950 rpm for 24 h in M9 medium containing nPET at a final concentration of 1.3 mg/ml and cells at an initial optical density $(OD)_{600}$ of 0.1. Values for strain S1 grown under the conditions shown in Figure 3F in the main text are included for comparison. The values (unprocessed data available in Data S1G) are the means of three biological replicates (n = 3), with standard deviations calculated using the STDEV. S function in Excel 2019. Figure created using the R programming language v.4.4.1, with core-base functions and in-house scripts. Abbreviation: T, terephthalic acid.

The genome-rewired *E. coli* matched the performance of these PET-degrading native strains, which illustrate, but do not represent, the full known diversity of PET-degrading microorganisms.

Integrating GenRewire with metabolic engineering for nPET upcycling

To further explore whether the engineered S1 strain could also introduce new opportunities for the use of *E. coli* as a producer of valuable chemical building blocks from nPET, we cloned *tph*A2, *tph*A3, *tph*B, and *tph*A1, which are part of an operon in *Comamonas thiooxidans* S23 encoding enzymes that convert T into PCA, into the plasmid pBBR1MCS (see STAR★METHODS). The plasmid was then heterologously introduced into the *E. coli* strain S1, resulting in strain $S1_{PCA}$ (with pBBR1MCS:*tph*A2A3BA1), which has the potential to produce PCA. Strain $S1_{PCA}$ was cultured in LB medium supplemented with T at a concentration of 10 mM to verify that it can metabolize T and convert it into PCA. Monitoring of the culture products by HPLC analysis confirmed the formation of PCA, demonstrating that the cluster is functional in *E. coli* strain $S1_{PCA}$ (Data S1H and Table S5 in the supplemental information online).

Once the functionality of the cluster was confirmed, we evaluated whether the engineered *E. coli* strain, which combines genetic reprogramming via GenRewire, CRISPR/Cas9 editing, and metabolic pathway incorporation, could efficiently degrade and utilize nPET as a carbon source for the biosynthesis of valuable compounds. To assess this, the $S1_{PCA}$ strain was cultured in M9 minimal medium supplemented with nPET. In brief, the cultures were grown in M9 medium supplemented with 25 μg/ml chloramphenicol (Cm), 100 μg/ml ampicillin (Amp), 1 mM isopropyl β-D-1-thiogalactopyranoside (IPTG), 0.1 mg/ml glycerol, and nPET particles at a final concentration of 1.3 mg/ml. Cultivation was initiated at an OD_{600nm} of 0.1 and carried out at 37°C for up to 20 h. Monitoring the culture OD_{600nm} values and biochemical transformations demonstrated that, when nPET was used as the sole carbon source, the $S1_{PCA}$ strain efficiently degraded the particles, reaching a total concentration of degradation products of 6942 ± 46 μM after 20 h (Figure 6A; Data S1H in the supplemental information online). It was also capable of growing by using the resulting E as a carbon source, as indicated by the OD_{600nm} reaching ~0.75 ± 0.01 after 20 h (Figure 6B; Data S1H). Finally, it was able to produce PCA at concentrations that, under the experimental conditions used, reached 4501 ± 45 μM at 20 h (Figure 6A; Data S1H). The data presented in Figure 6A indicate that the production of T and its subsequent conversion to PCA occur concurrently, as evidenced by the progressive increase in their concentrations.

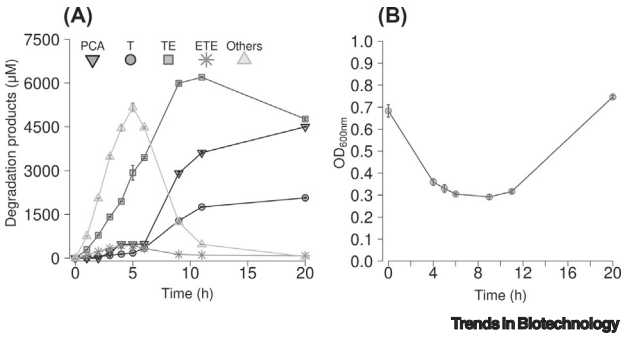

Figure 6. Bioconversion of polyethylene terephthalate nanoparticles (nPET) to valuable chemical precursors by genome-rewired and further engineered *Escherichia coli* strains. (A) Concentrations of degradation products (PET oligomers) and metabolic products (protocatechuate; PCA) during *in vivo* culture of the $S1_{PCA}$ strain in the presence of nPET. The cultivation conditions were as follows: M9 medium supplemented with 25 μg/ml chloramphenicol (Cm), 100 μg/ml ampicillin (Amp), 1 mM IPTG, and 0.1 mg/ml glycerol; initial optical density $(OD)_{600nm}$ of 0.1; 37°C; nPET particle concentration, 1.3 mg/ml; and incubation for 20 h (for details, see STAR★METHODS). Degradation products quantified by HPLC. (B) Follow-up of the OD_{600nm} of strain $S1_{PCA}$ under the conditions in (A). In all cases, values (unprocessed data available in Data S1H in the supplemental information online) represent the means of three biological replicates (n = 3), with standard deviations calculated using the STDEV function in Excel 2019. Figure created using the R programming language v.4.4.1, which uses core-base functions and in-house scripts. Abbreviation: T, terephthalic acid.

However, complete conversion of the degradation products to T, and subsequently to PCA, was not achieved within the 20-h timeframe, because a substantial amount of TE remained unconverted under the assay conditions.

Discussion

Here, we introduce GenRewire, a novel method for engineering bacterial strains to perform rationally designed biotechnological tasks. As a proof of concept, we endowed an *E. coli* strain, BL21 (DE3), with the ability to degrade nPET and use this environmentally harmful polymer for the production of safe biomass and for the efficient, sustainable production of chemicals (Video S2 in the supplemental information online). Until recently, PET degradation has been largely limited to the use of native microorganisms or microbial communities that contain native genes specialized in PET hydrolysis [36,37], as well as engineered microbes [38,39] or synthetic microbial consortia [40,41] that are equipped with foreign genes to carry out these biotechnological tasks. These approaches leverage synthetic biology tools to optimize expression and secretion plasmids, including surface display platforms [42,43] and conjugative systems [44], to deliver recombinant PET-degrading enzymes to a broad range of bacterial hosts. In our work, we successfully reprogrammed *E. coli* to efficiently depolymerize nPET. For this purpose, we did not need to introduce foreign genes encoding PET-hydrolyzing enzymes but instead repurposed *E. coli* proteins, none of which can degrade PET in their native state, without compromising microbial fitness.

This was first demonstrated through molecular modeling, which revealed that *E. coli* proteins that met specific criteria can harbor potential binding sites for PET substrates and can be reprogrammed into catalytic centers for PET depolymerization. Our study further demonstrates that it is possible to repurpose native *E. coli* proteins for PET degradation, specifically for degrading PET powder at temperatures between 37°C and 60°C. Nevertheless, there remains significant room for improvement, as the current degradation capacity does not yet match that of specialized and optimized benchmark PETase variants, such as LCC-ICCG [25] and HotPETase [26], and the conditions used in this study differ significantly from those optimal for large-scale hydrolysis [27]. However, outperforming these enzymes was not the primary objective of this study. Of the 23 variants sent for experimental validation, eight wild-type proteins and their reprogrammed variants were successfully expressed. Among these, three showed activity relevant to PET hydrolysis: one exhibited BHETase activity, as determined by the hydrolysis of ETE, and two displayed both BHETase and PETase activity, as confirmed by *in vitro* assays using PET powder. These results demonstrate the feasibility of repurposing *E. coli* proteins for PET degradation and further support the robustness of the methodology implemented in this study to confer this function to proteins that do not naturally have it.

While three out of eight proteins represents a good hit rate, the lack of activity in the remaining variants may be attributed to several factors. First, mutations can disrupt structural integrity, preventing proper folding of proteins. Notably, our MD simulations were not comprehensive and aimed to filter only the local triad environment, assuming overall integrity. To improve our pipeline, we will implement additional evolutionary constraints in the catalytic triad design, thereby reducing the likelihood of introducing disruptive changes that could impair partial protein folding. The solvent (and substrate) accessibility of the catalytic triad, particularly of the catalytic serine residue, could be another reason. Some of the noncatalytic variants displayed a catalytic triad predicted to be more buried, as calculated by their solvent accessible surface area (SASA) ($YfaP_m$, 16.9 Å^2; $Yfap_{m2}$, 24.3 Å^2; Fim_A, 11.7 Å^2; $YbiS_m$, 27.6 Å^2; and $YbiS_{m.2}$, 11.5 Å^2), compared with that of the variants showing activity ($SsuA_m$, 36.9 Å^2; $LsrB_m$, 20.2 Å^2; and $YggN_m$, 23.3 Å^2) [45]. In a subsequent series of designs, we plan to introduce an additional design step to strategically position a residue in the optimal location to function as an oxyanion hole.

Moreover, recent AI tools, such as proteinMPNN and PLACER, which are developed to predict protein stability and active-site preorganization, have been shown to increase success in engineering of enzymes (including serine hydrolases) [15]. Preliminary results from preprint studies further support their potential effectiveness in this context [46,47]. Integrating such tools and applying additional criteria to address the issues detected in this first analysis will facilitate higher success rates in PETase design efforts guided by the PluriZyme concept.

The second validation step demonstrated that nPET can be deconstructed *in vivo* by an *E. coli* strain engineered through genome rewiring and CRISPR/Cas9 editing, in which a single endogenous protein was modified to replace its native version without introducing foreign DNA. Although not intended to compete with specialized PET degraders, whether native or engineered (Figure 5 and Table S4), these results confirm the feasibility of our strategy to confer PET biodegradation capabilities on *E. coli*, a microorganism that does not naturally have this function. The observed activities are clearly meaningful, demonstrating that *E. coli* can be endowed with measurable PET-degrading capacity.

The innovative approach presented herein holds potential beyond PET degradation applications, highlighting its versatility when combined with complementary metabolic engineering tools. Validation revealed that, following the introduction of heterologous genes for E metabolism and T-to-PCA conversion, the genome-rewired and CRISPR-edited *E. coli* strain not only produced E and T from nPET, but also safely channeled them into the formation of biomass ($OD_{600\ nm}$ 1.33 ± 0.02, 20 h, 37°C) and the value-added compound PCA (4501 ± 45 μM, 20 h, 37°C). Although biological PET-to-T-to-PCA conversion using specialized engineered strains has been previously demonstrated and we did not aim to compete with such systems (Table S6 in the supplemental information online), our approach presents a notable distinction. Existing methods depend on externally generated T-enriched PET hydrolysates produced via chemical depolymerization [48], supplementation with purified PETases [49,50], or heterologous PETase expression in the engineered host [48]. This process can be streamlined by minimizing reliance on foreign DNA, which is commonly used to introduce heterologous PET-degrading functions, through the GenRewire strategy without compromising cellular growth or fitness. This represents a key advance since efficient bioconversions, including PET biodegradation and upcycling, demand strains where growth, substrate utilization, and performance are tightly coupled. This is usually achieved through labor-intensive design [7,51–54] and is often hindered by the inherent difficulty of expressing foreign proteins [51]. For example, an engineered *Clostridium* strain producing genome-integrated LCC or LCC-HFB7 showed lower PET degradation efficiency compared with strains expressing LCC or LCC-HFB7 from plasmids [55].

Our proof-of-concept study shows that GenRewire did not impair fitness under the tested conditions, although we did not address its stability over extended timescales. By replacing native genes with orthogonal variants that preserve the original function while introducing new catalytic activities, GenRewire maintains metabolic integrity and avoids perturbing core cellular processes. This orthogonal design minimizes unintended interference with native pathways, although minor resource competition may occur. In the absence of selective pressure, we expect the phenotype to be stable in the short-to-medium term; however, long-term evolutionary dynamics, including potential mutation accumulation, would require dedicated monitoring, such as periodic genome resequencing, to assess trait persistence in industrial or environmental settings.

Our approach involves the use of AI and physics-based methods; this would not be possible, for example, without the latest developments in AI deep learning structural prediction methods, from which one can readily obtain most of the bacterial protein folds. Our approach also uses state-of-

the-art molecular modeling software, the PELE Monte Carlo algorithm, which is capable of quickly mapping the protein–ligand interaction energy landscape and coupling it with hundreds of different mutations. Such an effort is possible only by the use of extensive parallel computational resources, such as those provided by supercomputers or cloud computing. With these appropriate tools, combined with the powerful capabilities of CRISPR/Cas9 genome editing, the microbial designs presented here can be achieved within 2–3 months.

Concluding remarks

This proof-of-concept study introduces GenRewire as a novel genome rewiring and editing method that, by applying the PluriZyme concept, enabled us to engineer *E. coli* to degrade nPET without the need for foreign DNA, which is commonly used to introduce heterologous PETases, and without compromising native cellular fitness. Through the combined use of deep learning-guided protein engineering and CRISPR-based genome editing, we show that native *E. coli* proteins, which are selected on the basis of defined criteria, can be computationally reprogrammed to exhibit artificial catalytic activity, notably enabling PET degradation. This outcome highlights the power of GenRewire: it enabled the design of a genome-rewired *E. coli* strain capable of deconstructing nPET without the need for exogenous catalytic or regulatory elements. Moreover, when complemented with a minimal set of foreign genes, the strain acquired upcycling capabilities. These results demonstrate that GenRewire enables the integration of new functions, such as PET degradation, as exemplified in this study, and reduces the reliance on foreign genetic material to perform complex bioconversions, as shown by our ability to produce PCA from nPET without introducing heterologous PETases.

We anticipate that this method will be readily applicable to other genomes and microbial chassis, given the nature of the computational and genome-editing tools used (see Outstanding questions). The application of this method to real systems based on PET powder will, in the future, enable us to assess the versatility of the method, the potential of genome-rewired strains for PET biodegradation and upcycling, and their scalability (see Outstanding questions). For example, degradation of PET powder was not achieved in this study, because the engineered variants are periplasmic-facing inner membrane proteins, which cannot access bulk PET powder but can act on nPET, which were used here solely to validate the proof-of-concept method developed in this work. Current efforts are directed toward designing variants of extracellular or surface-exposed membrane proteins, with the goal of enabling *E. coli* to degrade PET powder. Moreover, the continued integration of AI and molecular modeling is expected to refine the precision and efficiency of protein reprogramming, thereby optimizing both the design speed and catalytic output of next-generation engineered strains. GenRewire also opens the possibility of extending these designs to other bioconversions, given the adaptable nature of the computational tools, which can be tailored to act on selected substrates, not limited to PET-based substrates, as demonstrated in this proof-of-concept study.

STAR★METHODS

Detailed methods are provided in the online version of this paper and include the following:

- KEY RESOURCES TABLE
- EXPERIMENTAL MODEL AND STUDY PARTICIPANT DETAILS
  - Bacterial strains and growth conditions
- METHOD DETAILS
  - Structure generation, binding site scanning, molecular dynamics simulations
    - Computational proteome filtering
    - AlphaFold and PELE global explorations
    - Triad design

Outstanding questions

To what extent can the *Escherichia coli* genome be strategically rewired to enable efficient degradation and upcycling of PET powder?

How versatile is the GenRewire method across different microbial chassis beyond *E. coli*, and what are the main limitations when adapting it to alternative hosts?

How stable are GenRewire-engineered traits over time, and what evolutionary dynamics might affect their persistence without selective pressure in real-world applications?

How can AI and deep learning be further refined to improve the accuracy and versatility of GenRewire, enabling its application across diverse enzyme design efforts, including PETase engineering?

Can a microbial chassis genome be rewired to expose more than one enzyme of different classes, for example, allowing for cascade reactions?

  - Local refinement
  - Molecular dynamics
- Production of native proteins and variants
- Expression of LCC-ICCG and HotPETase
- Synthesis and expression of AldA and FucO
- ETE hydrolysis assays
- Production of nPET
- *In vitro* assays for PET hydrolysis
- CRISPR/Cas9 genome editing and heterologous expression of *fucO* & *aldA*
- *In vivo* cultures in the presence of nPET
- Analysis of degradation products by HPLC
- Analysis of degradation products by mass spectrometry (ESI/MS)
- Analysis of nPET by AFM and SEM
- Growth and fitness analysis
- *In vivo* degradation of nPET by native bacterial strains
- Cloning of the *tph*A2A3BA1 gene cluster from *C. thiooxidans* S23 for T catabolism
- Verification of T-to-PCA conversion in engineered *E. coli* strain

- QUANTIFICATION AND STATISTICAL ANALYSIS

RESOURCE AVAILABILITY

Lead contact

Further information and requests for resources and reagents should be directed to, and will be fulfilled by, the lead contact, Manuel Ferrer (mferrer@icp.csic.es) and Víctor Guallar (victor.guallar@bsc.es).

Materials availability

Plasmids and the engineered strains generated in this paper are available upon request from the lead contact. This study did not generate additional new unique reagents.

Data and code availability

The data that support the findings of this study are provided in the main text, supplemental information, and datasets.

The Molecular Dynamics Simulations have been deposited at Zenodo under the identifier https://zenodo.org/records/12568116. To use the archive, download the file, and extract its contents to a local directory using appropriate software. The directory contains separate folders for each type of simulation, along with input, output and README files. The unprocessed MS files and HPLC data have been deposited at Zenodo under the identifier https://zenodo.org/records/15784230. The directory contains separate folders for each type of data, and README files. Any additional information required to reanalyze the data reported in this paper is available from the lead contact upon request.

Author contributions

Conceptualization was led by V.G. and M.F. Methodology was developed by P.V., L.F-L., D.A., J.G-D., S.Rom., M.L., M.M-S., A.R-M., S.A.N., L.K., J.L.G-A., M.Fl., S.Rod., and P.P-G. Investigation was carried out by P.V., L.F-L., and D.A. Visualization efforts were contributed by J.G-D., S.Rom., M.F., M.L., M.M-S., A.R-M., S.A.N., R.B., and V.G. Supervision was provided by V.G., M.F., F.J.P., and P.S. Writing of the original draft was undertaken by V.G., L.F-L., and M.F., while review and editing were handled by V.G., M.F., P.S., P.V., L.F-L., J.L.G-A., P.P-G., W.R.S., and K.E.J.

Acknowledgments

M.F., V.G., P.S., P.P.G., W.R.S., and K.E.J. thank the European Union's Horizon 2020 Research and Innovation Programme for grant 101000327-FuturEnzyme, as well as Horizon Europe for grant 101060625-Nymphe (M.F.). Authors also acknowledge funding from the Ministerio de Ciencia, Innovación y Universidades, Agencia Estatal de Investigación (AEI) (MICIU/AEI/10.13039/501100011033), FEDER, EU, and the European Union NextGenerationEU/PRTR, supporting projects PID2020-

112758RB-I00 (M.F.), PDC2021-121534-I00 (M.F.), TED2021-130544B-I00 (M.F.), PID2023-153370OB-100 (M.F.), PID2019-106370RB-I00 (V.G.), and PID2022-136367OB-C31 (F.J.P.). In addition, they appreciate funding from the Spanish Ministry of Science and Innovation grant PRE2020-091825 (A.R-M.), and from the European Union's HORIZON-MSCA-2022-PF-01 programme grant 101104264-BIO DEGRADE (J.G-D.). Funding from the 'César Nombela' Research Talent Attraction Program, grant 2024-T1/ECO-31227 from the Consejería de Educación, Ciencia y Universidades de la Comunidad de Madrid (R.B.), is also gratefully acknowledged. M.Fl. acknowledges his AI4S fellowship within the "Generación D" initiative by Red.es, Ministerio para la Transformación Digital y de la Función Pública, for talent attraction (C005/24-ED CV1), funded by NextGenerationEU through PRTR. The authors extend their gratitude to Rebecka Molitor for her support with native strains. We also thank Alan Wypych and Robert F. Dierkes for kindly donating the plasmid carrying the *Comamonas* genes for T-to-PCA conversion.

Declaration of interests

The authors declare no competing interests.

Supplemental information

Supplemental information associated with this article can be found online at https://doi.org/10.1016/j.tibtech.2025.07.008.

References

1. Marx, V. (2023) Method of the year: long-read sequencing. *Nat. Methods* 20, 6–11
2. Cervantes-Gracia, K. *et al.* (2022) Integrative OMICS data-driven procedure using a derivatized meta-analysis approach. *Front. Genet.* 13, 828786
3. Jumper, J. *et al.* (2021) Highly accurate protein structure prediction with AlphaFold. *Nature* 596, 583–589
4. van Kempen, M. *et al.* (2024) Fast and accurate protein structure search with Foldseek. *Nat. Biotechnol.* 42, 243–246
5. Alonso, S. *et al.* (2020) Genetically engineered proteins with two active sites for enhanced biocatalysis and synergistic chemo- and biocatalysis. *Nat. Catal.* 3, 319–328
6. Robles-Martín, A. *et al.* (2023) Sub-micro- and nano-sized polyethylene terephthalate deconstruction with engineered protein nanopores. *Nat. Catal.* 6, 1174–1185
7. Yilmaz, S. *et al.* (2022) Towards next-generation cell factories by rational genome-scale engineering. *Nat. Catal.* 5, 751–765
8. Fu, J. *et al.* (2024) Reprogramming *Yarrowia lipolytica* metabolism for efficient synthesis of itaconic acid from flask to semipilot scale. *Sci. Adv.* 10, eadn0414
9. Li, Y. *et al.* (2015) Metabolic engineering of *Escherichia coli* using CRISPR-Cas9 meditated genome editing. *Metab. Eng.* 31, 13–21
10. Watson, J.L. *et al.* (2023) *De novo* design of protein structure and function with RFdiffusion. *Nature* 620, 1089–1100
11. Dauparas, J. *et al.* (2022) Robust deep learning-based protein sequence design using ProteinMPNN. *Science* 378, 49–56
12. Madani, A. *et al.* (2023) Large language models generate functional protein sequences across diverse families. *Nat. Biotechnol.* 41, 1099–1106
13. Hong, L. and Kortemme, T. (2024) An integrative approach to protein sequence design through multiobjective optimization. *PLoS Comput. Biol.* 20, e1011953
14. Yeh, A.H. *et al.* (2023) *De novo* design of luciferases using deep learning. *Nature* 614, 774–780
15. Lauko, A. *et al.* (2025) Computational design of serine hydrolases. *Science* 388, eadu2454
16. Santiago, G. *et al.* (2018) Rational engineering of multiple active sites in an ester hydrolase. *Biochemistry* 57, 2245–2255
17. Robles-Martín, A. *et al.* (2024) Behind the scenes of *PluriZyme* designs. *Eng* 5, 91–103
18. Roda, S. *et al.* (2022) A *Plurizyme* with transaminase and hydrolase activity catalyzes cascade reactions. *Angew. Chem. Int. Ed.* 61, e202207344
19. Almagro Armenteros, J.J. *et al.* (2019) SignalP 5.0 improves signal peptide predictions using deep neural networks. *Nat. Biotechnol.* 37, 420–423
20. Hallgren, J. *et al.* (2022) DeepTMHMM predicts alpha and beta transmembrane proteins using deep neural networks. *bioRxiv*, Published online April 10, 2022. https://doi.org/10.1101/2022.04.08.487609
21. Berman, H.M. *et al.* (2000) The Protein Data Bank. *Nucleic Acids Res.* 28, 235–242
22. Burley, S.K. *et al.* (2023) RCSB Protein Data Bank (RCSB.org): delivery of experimentally-determined PDB structures alongside one million computed structure models of proteins from artificial intelligence/machine learning. *Nucleic Acids Res.* 51, 488–508
23. Varadi, M. *et al.* (2022) AlphaFold Protein Structure Database: massively expanding the structural coverage of protein-sequence space with high-accuracy models. *Nucleic Acids Res.* 50, 439–444
24. Schubert, S. *et al.* (2023) Reaction pathways for the enzymatic degradation of poly(ethylene terephthalate): what characterizes an efficient PET-hydrolase? *ChemBioChem* 24, e202200516
25. Tournier, V. *et al.* (2020) An engineered PET depolymerase to break down and recycle plastic bottles. *Nature* 580, 216–219
26. Bell, E.L. *et al.* (2022) Directed evolution of an efficient and thermostable PET depolymerase. *Nat. Catal.* 5, 673–681
27. Arnal, G. *et al.* (2023) Assessment of four engineered PET degrading enzymes considering large-scale industrial applications. *ACS Catal.* 13, 13156–13166
28. Białas, N. *et al.* (2022) Bacteria (*E. coli*) take up ultrasmall gold nanoparticles (2 nm) as shown by different optical microscopic techniques (CLSM, SIM, STORM). *Nano Select* 3, 1407–1420
29. Brito, P.H. *et al.* (2013) Natural genome diversity of AI-2 quorum sensing in *Escherichia coli*: conserved signal production but labile signal reception. *Genome Biol. Evol.* 5, 16–30
30. Miller, S.T. *et al.* (2024) *Salmonella typhimurium* recognizes a chemically distinct form of the bacterial quorum-sensing signal AI-2. *Mol. Cell* 15, 677–687
31. Beale, J. *et al.* (2010) Structure of the aliphatic sulfonate-binding protein SsuA from *Escherichia coli*. *Acta Crystallogr. Sect. F Struct. Biol. Cryst. Commun.* 66, 391–396
32. Panda, S. *et al.* (2021) Improving ethylene glycol utilization in *Escherichia coli* fermentation. *Biochem. Eng. J.* 168, 107957
33. Pandit, A.V. *et al.* (2021) Engineering *Escherichia coli* for the utilization of ethylene glycol. *Microb. Cell Factories* 20, 22
34. Yang, D.D. *et al.* (2024) Synonymous edits in the *Escherichia coli* genome have substantial and condition-dependent effects on fitness. *Proc. Natl. Acad. Sci. U. S. A.* 121, e2316834121
35. Kruse, L. *et al.* (2024) *Halopseudomonas* species: cultivation and molecular genetic tools. *Microb. Biotechnol.* 17, e14369
36. Joo, S. *et al.* (2018) Structural insight into molecular mechanism of poly(ethylene terephthalate) degradation. *Nat. Commun.* 9, 382
37. Barreto Roman, E.K. *et al.* (2024) Plastic-degrading microbial communities reveal novel microorganisms, pathways, and

biocatalysts for polymer degradation and bioplastic production. *Sci. Total Environ.* 949, 174876
38. Tiso, T. *et al.* (2022) The metabolic potential of plastics as biotechnological carbon sources – review and targets for the future. *Metab. Eng.* 71, 77–98
39. Satta, A. *et al.* (2024) Metabolic and enzymatic engineering strategies for polyethylene terephthalate degradation and valorization. *Rev. Environ. Sci. Biotechnol.* 23, 351–383
40. Bao, T. *et al.* (2023) Engineering microbial division of labor for plastic upcycling. *Nat. Commun.* 14, 5712
41. Jiménez, D.J. *et al.* (2025) Engineering the mangrove soil microbiome for selection of polyethylene terephthalate-transforming bacterial consortia. *Trends Biotechnol.* 43, 162–183
42. Jia, Y. *et al.* (2022) Hydrophobic cell surface display system of PETase as a sustainable biocatalyst for PET degradation. *Front. Microbiol.* 13, 1005480
43. Xue, K. *et al.* (2024) Bacterial surface display of PETase mutants and MHETase for an efficient dual-enzyme cascade catalysis. *Bioresour. Technol.* 408, 131177
44. Yip, A. *et al.* (2024) Degradation of polyethylene terephthalate (PET) plastics by wastewater bacteria engineered via conjugation. *Microb. Biotechnol.* 17, e70015
45. Fraczkiewicz, R. and Braun, W. (1998) Exact and efficient analytical calculation of the accessible surface areas and their gradients for macromolecules. *J. Comput. Chem.* 19, 319–333
46. Anishchenko, I. *et al.* (2024) Modeling protein-small molecule conformational ensembles with ChemNet. *bioRxiv*, Published online September 25, 2024. https://doi.org/10.1101/2024.09.25.614868
47. Kim, D. *et al.* (2025) Computational design of metallohydrolases. *bioRxiv*, Published online April 11, 2025. https://doi.org/10.1101/2024.11.13.623507
48. Werner, A.Z. *et al.* (2021) Tandem chemical deconstruction and biological upcycling of poly(ethylene terephthalate) to β-ketoadipic acid by *Pseudomonas putida* KT2440. *Metab. Eng.* 67, 250–261
49. Sadler, J.C. and Wallace, S. (2021) Microbial synthesis of vanillin from waste poly(ethylene terephthalate). *Green Chem.* 13, 4665–4672
50. Diao, J. *et al.* (2023) Upcycling of poly(ethylene terephthalate) to produce high-value bio-products. *Cell Rep.* 42, 111908
51. Ceroni, F. *et al.* (2015) Quantifying cellular capacity identifies gene expression designs with reduced burden. *Nat. Methods* 12, 415–418
52. Pontrelli, S. *et al.* (2018) *Escherichia coli* as a host for metabolic engineering. *Metab. Eng.* 50, 16–46
53. Gao, H. *et al.* (2024) Recent advances in genome-scale engineering in *Escherichia coli* and their applications. *Eng. Microbiol.* 4, 100115
54. Orsi, E. *et al.* (2021) Growth-coupled selection of synthetic modules to accelerate cell factory development. *Nat. Commun.* 12, 5295
55. Liu, Y.-J. *et al.* (2025) Optimized whole-cell depolymerization of polyethylene terephthalate to monomers using engineered *Clostridium thermocellum*. *J. Hazard. Mater.* 488, 137441
56. Jeong, H. *et al.* (2015) Complete genome sequence of *Escherichia coli* strain BL21. *Genome Announc.* 3, e00134-15
57. The UniProt Consortium (2023) UniProt: the Universal Protein Knowledgebase in 2023. *Nucleic Acids Res.* 51, 523–531
58. Kaushik, S. *et al.* (2022) Bacterial signal peptides: navigating the journey of proteins. *Front. Physiol.* 13, 933153
59. Nielsen, H. *et al.* (2019) A brief history of protein sorting prediction. *Protein J.* 38, 200–216
60. Sastry, G.M. *et al.* (2013) Protein and ligand preparation: parameters, protocols, and influence on virtual screening enrichments. *J. Comput. Aided Mol. Des.* 27, 221–234
61. Borrelli, K.W. *et al.* (2005) PELE: Protein Energy Landscape Exploration. A novel Monte Carlo based technique. *J. Chem. Theory Comput.* 1, 1304–1311
62. Lecina, D. *et al.* (2017) Adaptive simulations, towards interactive protein-ligand modeling. *Sci. Rep.* 7, 8466
63. Díaz, L. *et al.* (2020) Monte Carlo simulations using PELE to identify a protein-protein inhibitor binding site and pose. *RSC Adv.* 10, 7058–7064
64. Banks, J.L. *et al.* (2005) Integrated Modeling Program, Applied Chemical Theory (IMPACT). *J. Comput. Chem.* 26, 1752–1780
65. Nivón, L.G. *et al.* (2013) A pareto-optimal refinement method for protein design scaffolds. *PLoS ONE* 8, e59004
66. Conway, P. *et al.* (2014) Relaxation of backbone bond geometry improves protein energy landscape modeling. *Prot. Sci.* 23, 47–55
67. Alford, R.F. *et al.* (2017) The Rosetta all-atom energy function for macromolecular modeling and design. *J. Chem. Theory Comput.* 13, 3031–3048
68. Abraham, M.J. *et al.* (2015) GROMACS: high performance molecular simulations through multi-level parallelism from laptops to supercomputers. *SoftwareX* 1, 19–25
69. Páll, S. *et al.* (2015) Tackling Exascale software challenges in molecular dynamics simulations with GROMACS. *Lect. Notes Comput. Sci* 8759, 3–27
70. Lindorff-Larsen, K. *et al.* (2010) Improved side-chain torsion potentials for the Amber ff99SB protein force field. *Proteins* 78, 1950–1958
71. Jorgensen, W.L. *et al.* (1983) Comparison of simple potential functions for simulating liquid water. *J. Chem. Phys.* 79, 926–935
72. Sousa da Silva, A.W. and Vranken, W.F. (2012) ACPYPE - AnteChamber PYthon Parser interfacE. *BMC Res. Notes* 5, 367
73. Jakalian, A. *et al.* (2002) Fast, efficient generation of high-quality atomic charges. AM1-BCC model: II. Parameterization and validation. *J. Comput. Chem.* 23, 1623–1641
74. He, X. *et al.* (2020) A fast and high-quality charge model for the next generation general AMBER force field. *J. Chem. Phys.* 153, 114502
75. Andersen, H.C. (1980) Molecular dynamics simulations at constant pressure and/or temperature. *J. Chem. Phys.* 72, 2384–2393
76. Parrinello, M. and Rahman, A. (1981) Polymorphic transitions in single crystals: A new molecular dynamics method. *J. Appl. Phys.* 52, 7182–7190
77. Darden, T. *et al.* (1993) Particle mesh Ewald: an N·log(N) method for Ewald sums in large systems. *J. Chem. Phys.* 98, 10089–10092
78. Essmann, U. *et al.* (1995) A smooth particle mesh Ewald method. *J. Chem. Phys.* 103, 8577–8593
79. Feenstra, K.A. *et al.* (1999) Improving efficiency of large time-scale molecular dynamics simulations of hydrogen-rich systems. *J. Comput. Chem.* 20, 786–798
80. Hess, B. *et al.* (1997) LINCS: a linear constraint solver for molecular simulations. *J. Comput. Chem.* 18, 1463–1472
81. Hess, B. (2008) P-LINCS: a parallel linear constraint solver for molecular simulation. *J. Chem. Theory Comput.* 4, 116–122
82. Hockney, R.W. *et al.* (1974) Quiet high-resolution computer models of a plasma. *J. Comput. Phys.* 14, 148–158
83. McGibbon, R.T. *et al.* (2015) MDTraj: a modern open library for the analysis of molecular dynamics trajectories. *Biophys. J.* 109, 1528–1532
84. Hunter, J.D. (2007) Matplotlib: a 2D graphics environment. *Comput. Sci. Eng.* 9, 90–95
85. Waskom, M.L. (2021) Seaborn: statistical data visualization. *J. Open Source Softw.* 6, 3021
86. Laemmli, U. (1970) Cleavage of structural proteins during the assembly of the head of Bacteriophage T4. *Nature* 227, 680–685
87. Bradford, M.M. (1976) A rapid and sensitive method for the quantitation of microgram quantities of protein utilizing the principle of protein-dye binding. *Anal. Biochem.* 72, 248–254
88. Dawson, A. and Kamat, P.V. (2000) Complexation of gold nanoparticles with radiolytically generated thiocyanate radicals ($(SCN)_2^{\bullet-}$). *J. Phys. Chem. B* 104, 11842–11846
89. Dawson, A. and Kamat, P.V. (2001) Semiconductor–metal nanocomposites. Photoinduced fusion and photocatalysis of gold-capped TiO_2 (TiO_2/Gold) nanoparticles. *J. Phys. Chem. B* 105, 960–966
90. Perez-Garcia, P. *et al.* (2023) An archaeal lid-containing feruloyl esterase degrades polyethylene terephthalate. *Commun. Chem.* 6, 193
91. Kasai, D. *et al.* (2010) Transcriptional regulation of the terephthalate catabolism operon in *Comamonas* sp. strain E6. *Appl. Environ. Microbiol.* 76, 6047–6055
92. Dierkes, R.F. *et al.* (2023) An ultra-sensitive *Comamonas thiooxidans* biosensor for the rapid detection of enzymatic polyethylene terephthalate (PET) degradation. *Appl. Environ. Microbiol.* 89, e01603-22

STAR★METHODS

KEY RESOURCES TABLE

Reagent or resource	Source	Identifier
Bacterial and virus strains		
E. coli BL21 (DE3)	Agilent Technologies, Inc.	200131
E. coli BL21 (DE3) (*lsrB*$_m$)	GenScript Biotech (Netherlands) B.V.	U062JMDUG0
Chemicals, peptides, and recombinant proteins		
Luria Bertani (LB) medium	ThermoFisher Scientific	12780029
LB agar medium	ThermoFisher Scientific	22700041
M9 minimal medium	Merck Life Science S.L.U.	M6030
Ampicillin	ThermoFisher Scientific	BP1760
Chloramphenicol	Merck Life Science S.L.U.	C0378
Kanamycin sulfate	SERVA Electrophoresis GmbH	26899
Isopropyl β-D-1-thiogalactopyranoside	ThermoFisher Scientific	302790250
L-Arabinose, ≥99% (GC)	Merck Life Science S.L.U.	A3256
Glycerol, ≥99.5% (GC)	Merck Life Science S.L.U.	49767
D-(+)-Glucose, ≥99.5%	Merck Life Science S.L.U.	G7021
NaH_2PO_4, 99-100,5%	Panreac Química S.L.U.	141677.1211
Na_2HPO_4, 99-102 %	Panreac Química S.L.U.	131678.1211
NaCl, ACS reagent, ≥99.0%	Merck Life Science S.L.U.	106404
Gold (III) chloride trihydrate ($HAuCl_4 \bullet 3H_2O$), ≥99.9%	Merck Life Science S.L.U.	520918
Sodium borohydride ($NaBH_4$), ≥98.0%	Merck Life Science S.L.U.	452882
4-(2-Hydroxyethyl)-1-piperazineethanesulfonic acid, 99%	ThermoFisher Scientific	BP310-5
Imidazole, ≥99.5% (GC)	Merck Life Science S.L.U.	56748
Bis(2-hydroxyethyl) terephthalate	Merck Life Science S.L.U.	465151
3,4-Dihydroxybenzoic acid, ≥97.0% (T)	Merck Life Science S.L.U.	37580
Solvent pre-treated amorphous PET	Goodfellow Cambridge	ES301445
PET powder (<300 μm, >40% crystallinity)	Goodfellow Cambridge	ES30-PD-000132
Impranil® DLN-SD emulsion	Covestro	https://solutions.covestro.com/en/products/impranil/impranil-dln-sd_000000000057821411
Silicon wafer	agar scientific	G3390
1,1,1,3,3,3-Hexafluor-2-propanole	Merck Life Science S.L.U.	105228
Formic acid, 85% w/w	Scharlab S.L.	AC1080
Acetonitrile, min. 99.9 %	Scharlab S.L.	AC0371
Dimethyl sulfoxide, 99,9%	Scharlab S.L.	SU01521000
Trifluoroacetic acid, purum, ≥98.0% (T)	Fluka	91700
Lysonase Bioprocessing reagent	Merck Life Science S.L.U.	71230
HIS-Select Nickel Affinity Gel	Merck Life Science S.L.U.	P6611
Amicon® Ultra-15 centrifugal filter unit,	Merck Life Science S.L.U.	UFC9010

(continued on next page)

(continued)

Reagent or resource	Source	Identifier
Regenerated cellulose membrane, MWCO 10 kDa		
Nylon syringe filter, 0.45 µm pore size, 13 mm diameter	Membrane Solutions	SFNY013045N
Syringe filters with acrylic housing sterile, 0.2 µm pore size, 25 mm diameter	VWR International Inc.	28145-501
Seeband protein staining solution	Gene Bio-Application Ltd.	SB010
Bio-Rad protein assay dye reagent concentrate	BioRad	500-006
Superdex 75 10/300 GL and 5/150 GL	Merck Life Science S.L.U.	GE17-5174-01
Zorbax Eclipse Plus C-18 (4.6 x 100 mm, 3.5 µm)	Agilent Technologies, Inc.	959961-902
Zorbax Eclipse XDB C-18 column (9.4 × 250 mm, 5 µm)	Agilent Technologies, Inc.	990967-202
Sunfire C18 RP precolumn (2.1 mm × 5 mm)	Waters	186002539
Atlantis T3 C18 RP column (2.1 mm × 100 mm)	Waters	186003718
Recombinant DNA		
pBBR1MCS::*tphA2A3BA1*	This paper	N/A
pET-21(+) plasmids	Twist Biosciences	Q-283367
pET-45b(+) plasmids	GenScript Biotech (Netherlands) B.V.	U1013145G0
Software and algorithms		
SignalP 5.0	DTU Health Tech	https://services.healthtech.dtu.dk/services/SignalP-5.0/
DeepTMHMM	Technical University of Denmark	https://dtu.biolib.com/DeepTMHMM
AlphaFold Protein Structure database	Google DeepMind	https://alphafold.ebi.ac.uk/
AlphaFold 2.0	Google DeepMind	https://alphafold.ebi.ac.uk/
Protein Preparation Wizard	Schrödinger	www.schrodinger.com/life-science/learn/white-papers/protein-preparation-wizard/
PELE Software (version 1.8.0), PELE Platform 1.6.3, AdaptivePELE version 1.7.1	Electronic and Atomic Protein Modeling (EAPM) group, BSC	https://pele.bsc.es/pele.wt https://nostrumbiodiscovery.github.io/pele_platform/# https://nostrumbiodiscovery.github.io/pele_docs/
Rosetta modeling software suite (release 337)	Rosetta Commons	https://rosettacommons.org/software/
GROMACS 2018	GROMACS	https://manual.gromacs.org/2018/index.html
Antechamber Python Parser interfacE (ACPYPE)	https://alanwilter.github.io/acpype/	www.bio2byte.be/acpype/
MDtraj	Stanford University	www.mdtraj.org/1.9.8.dev0/index.html
PyMOL	Schrödinger	www.pymol.org/
Matplotlib	Matplotlib	https://matplotlib.org/
Seaborn	Seaborn	https://seaborn.pydata.org/
WSxM free software package	WSxM	http://wsxm.eu/
ImageJ free software package	National Institutes of Health	https://imagej.net/ij/download.html
Varian Star LC workstation 6.41	Agilent Technologies, Inc.	www.agilent.com/library/usermanuals/public/914760.pdf
MassLynx V4.1	Waters	www.waters.com/webassets/cms/support/docs/71500113203ra.pdf
R programming environment	The R Foundation	www.r-project.org/
BioTek Gen5 2.0 software	Agilent Technologies, Inc.	www.agilent.com/en/product/microplate-instrumentation/microplate-

(continued)

Reagent or resource	Source	Identifier
		instrumentation-control-analysis-software/imager-reader-control-analysis-software/biotek-gen5-software-for-detection-1623227
Varian ProStar software	Varian Inc.	www.chromatography.varian.com.
Other		
Proteome database	UniProt	www.uniprot.org/
Burette	Afora S.A.	A-6055
Screw tube 15 ml, 120 x 17 mm	Sarstedt AG & Co.	62.554.502
Screw tube 50 ml, 114 x 28 mm	Sarstedt AG & Co.	62.547.254
2-ml Safe-lock polypropylene tubes	Eppendorf SE	0030120094
96-Well U-bottom microplate	Greiner Bio-One	650161
Vial of 2 ml clear 9-425 screw top	Membrane Solutions	LBSV022C
0.25 ml micro-insert, 31 x 6 mm, conical, clear glass, 15 mm top	Lab Logistic Group GmbH	7401744
3 Parts syringe without needle	Ico Plus 3	N14360
Vial caps, pre-slit blue PTFE/White silicone septa+ blue screw cap with hole, for 2 ml	Membrane Solutions	LBSV222CSS
Pur-A-LyzerTM Maxi 1200 dialysis kit	Merck Life Science S.L.U.	PURX60100
Rotapapor R-210	Buchi Ibérica S.L.U.	CH9230
Sonicator 3000	Misonix	M98820
Fast protein liquid chromatography (FPLC)	Amersham Bioscience	LCC-500CI
Mini PROTEAN electrophoresis system	Bio–Rad	041BR
MaxQ 6000 refrigerated incubator shaker	Thermo Fisher Scientific	T-MAXQ6
Centrifuge 5810 R	Eppendorf SE	581112714
Orbital incubator SI500	Stuart Scientific Co. Ltd	R000102971
BioPhotometer	Eppendorf SE	6131 25728
GenePulser Xcell™	Bio–Rad	1652667
Quaternary pump Model 1100	Agilent Technologies, Inc.	www.agilent.com/en/support/liquid-chromatography/a03681
Autosampler Model L-2200	Hitachi, Ltd.	890-0202
Photodiode array detector Varian ProStar	Varian Inc.	EL05059010

EXPERIMENTAL MODEL AND STUDY PARTICIPANT DETAILS

Bacterial strains and growth conditions

In this study, we used the bacterial strain *E. coli* BL21 (DE3). Unless otherwise indicated, all bacteria were grown in Luria–Bertani (LB) broth (Invitrogen, Thermo Fisher Scientific, MA, USA; ref. 12780029), LB agar (Invitrogen, Thermo Fisher Scientific, MA, USA; ref. 22700041), or minimal medium M9 (Merck Life Science S.L.U., Madrid, Spain; ref. M6030).

METHOD DETAILS

Structure generation, binding site scanning, molecular dynamics simulations

Computational proteome filtering. The genome sequence of *E. coli* strain BL21 (DE3) was obtained from the UniProt proteome database [56,57], which contains 4,156 protein sequences. We first filtered the proteins by sequence length, excluding proteins with less than 100 and more than 450 amino acids. Next, we applied additional filters to the proteins in order to classify them and prioritize non-membrane extracellular proteins. We employed scraping tools to gather the available protein information (if any) from the UniProt database [57]. The second filter applied was the subcellular localization of the proteins. However, not all proteins had this information available in the database. Therefore, we predicted the subcellular localization based on the presence of a signal peptide (SP) using SignalP5.0 [19], a bioinformatic tool based on deep convolutional and recurrent neural network algorithms. SP are short segments

of amino acids (15-30 residues) usually present at the N-terminus that are recognized by cytosolic proteins, and then inserted or translocated across the membrane [58,59]. As a result, its presence in a protein is key in determining if a protein is exported. We defined the presence of a signal peptide sequence if any of the predicted values from SignalP5.0 (Sec/SPI, Tat/SPI or Sec/SPII) were equal or higher than 0.6, and kept the proteins containing these sequences. Then, we applied a third filter and classified the proteins using DeepTMHMM [20], a deep learning tool for transmembrane topology prediction, into soluble or membrane proteins. The proteins predicted as membrane proteins were discarded as well.

AlphaFold and PELE global explorations. We retrieved the 3D crystal structures or models of the protein sequences from the RCSB PDB (RSCB.org) or the AlphaFold Protein Structure [21,22] database, respectively, if available, or running AlphaFold 2.0 [23]. AlphaFold models were filtered to remove those with average per-residue model confidence score (pLDDT) scores below 70. In addition, the N- and C-terminal domains of each model were removed if they had a pLDDT below 70. All remaining protein models were prepared with the Protein Preparation Wizard from Schrödinger [60] to fix protonation states at pH 7.5 and other common problems (missing side chains, atomic clashes, etc.). A substrate migration sampling of the models was performed to predict potential PET binding sites with the GE protocol of the PELE software [61–63]. PELE is an unconstrained ligand exploration technique employing Monte Carlo sampling. After substrate perturbation (translation and rotation), it uses an experimental rotamer library to predict the protein side- chain conformations within 6 angstroms of the substrate. Then, it performs a final minimization to generate a new pose. This new pose is accepted or rejected based on the Metropolis criterion. The OPLS2005 force field [64] was employed in the simulations to define the total and enzyme-substrate interaction energies at each step. The PELE GE protocol performs a dynamic exploration of the surface of the protein, placing 31 initial copies of the substrate around it and running 50 iterations (epochs) of 12 PELE steps in 32 CPUS (31 trajectories), searching for the best binding site for the substrate on the protein. We used three ligand models to perform the PELE GE: ETETETE, ETETE and TE. Then, we selected the best 100 proteins for each substrate ranked according to their enzyme-substrate interaction binding energy, compared them and selected the proteins that bind at least two substrates. Next, we checked whether the substrates bind at the same binding site, and discarded the proteins where the substrates bind at different locations. We verified with the available information of the models that the substrates were not located near known active sites, that is, if any atom of the substrates was located closer than 6 Å to any known catalytic residue. After discarding these proteins, we ended up with 25 proteins that bind at least 2 substrates at the same binding site.

Triad design. The selected proteins were individually relaxed using the fast relax protocol [65,66] of Rosetta Modeling Software. No constraints were used for the relaxations, which consisted of 5 relaxation cycles and 1000 independent trajectories. The poses with the best Rosetta score [67] from these optimizations were used for searching sites of triad insertion. Serine rotamers were tried numeratively every 20° for each residue position at close contact with the ligand's carbonyl-carbon atoms. All rotamers compatible with catalytic distances between serine and ligand were accepted, and neighbor positions to these serine positions were also tried for compatible histidine rotamers. Analogously, this was repeated to position an aspartic residue. From all geometrically compatible combinations of rotamers, the one with the lowest Rosetta score was selected for every unique triad found. All triads were relaxed using the fast relax protocol of Rosetta Modeling Software to remove possible clashes with the newly inserted residues. The relaxation was performed with constraints over the backbone and side chain heavy atom positions, with a ramping from full to zero in the first relax phase. Five relaxation cycles and 100 independent trajectories were generated, and the best-rosetta score pose was obtained for each model.

Local refinement. We simulated the proteins with the inserted catalytic triad with each substrate using the induced fit module of the PELE software. Two simulation rounds were made consecutively; the first round consisted of 100 steps, 5 iterations with 48 trajectories, and the second round was more resource-intense, with 100 steps, 10 iterations and 96 CPUs. The simulations of the first round were evaluated using a series of metrics describing the hydrolysis process, and the next round of PELE was started from the poses extracted from the first round with better binding energies that meet all the metric requirements. We used the following metrics to classify poses as catalytic: distance of the C atoms of the carbonyl group/s of the substrate to the O atom of the catalytic serine (Ser - Lig) below 5 Å, distance of the O atom of the catalytic serine to the deprotonated N atom of the catalytic histidine (Ser - His) below 3.5 Å, and distance of the protonated N atom of the catalytic histidine to the closest side chain O atom of the catalytic aspartic acid (His - Asp) below 3.5 Å.

Designed catalytic triads were filtered based on the results of their PELE scores before further assessment with molecular dynamics. We defined the catalytic binding free energy as the expectation value of the binding energy for catalytic poses based on a Boltzmann distribution and used it as the filtering score. First, the probabilities were assigned to each pose in the simulation based on a Boltzmann distribution:

$$P_i = \frac{e^{-E_i/KT}}{Q} \quad [1]$$

Here, Pi is the probability of the ith pose, Ei is its total energy, KT is the energy partition constant, and Q is the partition function for a simulation of N poses, defined as:

$$Q = \sum_{i}^{N} e^{-E_i/KT} \quad [2]$$

Finally, the above probabilities are used to integrate the individual binding energy values Eib of the catalytic poses of the simulation:

$$\langle E^b \rangle = \sum_{i}^{N} P_i E_i^b \quad [3]$$

Molecular dynamics. We used GROMACS 2018 [68,69] to simulate the whole system using AMBER99SB*_ILDN force field [70] for the protein and TIP3P for water molecules [71]. The ligands (ETETETE or ETETE) were parametrized using Antechamber Python Parser interfacE (ACPYPE) [72] with the AM1-BCC scheme [73], and the GAFF2 was used as the molecular force field [74]. The systems were neutralized with Na^+ and Cl^- ions and solvated in an octahedral TIP3P water box with a minimum distance of 10 Å between the protein and the box. The simulations were run at 298.15 K using an Andersen thermostat [75] and at 1 bar using the Parrinello-Rahman barostat [76] in the NPT ensemble with periodic boundary conditions and with Particle Mesh Ewald electrostatics [77,78]. Hydrogen repartitioning mass [79] was used with the LINCS algorithm [80,81], with constraints and reset of bonds between heavy and hydrogen atoms to allow an increased time step of the simulations of 4 fs. using a leap-frog integrator [82]. The system was equilibrated in the NVT ensemble from 10 K to 298.15 K along 100 ps with 10 kcal/(mol·Å^2) constraints on all bonds and then equilibrated in 10 consecutive 200 ps steps with decreased constraints (1000, 550, 300, 170, 90, 50, 30, 15, 10, 5 kcal/(mol·Å^2)). Two replicas of 200 ns were run for each system. The same protocol was applied to wild-type PETase proteins as a positive control (PDB codes: 5XGO (https://www.ncbi.nlm.nih.gov/Structure/pdb/5XGO), 6ANE (https://www.ncbi.nlm.nih.gov/Structure/pdb/6ANE) and 5XJH (https://www.ncbi.nlm.nih.gov/Structure/pdb/5XJH)). The simulations were analyzed using MDtraj [83], calculating the Ser - Lig, Ser - His, and His - Asp distances as defined before for all the simulation time. Selection of the best models to try experimentally was done according to the percentage of time (more than 35 %) that the catalytic triad stayed in a catalytic position throughout the simulation.

Heterogeneous modeling data were represented (Figure 2 in the main text) with PyMOL molecular viewer (Version 2.5 Schrödinger, LLC) and graphs with Python Matplotlib [84] and Seaborn libraries [85].

Production of native proteins and variants

Once identified, the amino acid sequences encoding the native proteins and variants (see accession numbers and sequences in Data S1A-B) were used as templates for gene synthesis. The sequences were synthesized by Twist Biosciences (San Francisco, CA, USA) and codon-optimized to maximize expression in *Escherichia coli*. In brief, before gene synthesis, the sequence was analyzed for the presence of a signal peptide using the SignalP-5.0 tool [19]. The gene, including the signal peptide, was flanked by BamHI and HindIII (stop codon) restriction sites and inserted into a pET-21(+) expression vector with an ampicillin selection marker (Twist Biosciences, San Francisco, CA, USA). This plasmid, which was introduced into *E. coli* BL21 (DE3), supports the expression of C-terminal His6-fusion proteins, with the final amino acid sequence of the synthetic protein being X- KLAAALEHHHHHH (where X corresponds to the original sequence of the target enzyme with the signal peptide). After synthesis, the soluble C-terminal His6-tagged proteins, native

and engineered variants, were produced using LB medium (ThermoFisher Scientific, MA, USA; ref. 12780029) and purified at >98% purity, as determined by SDS-PAGE analysis (Figures S1 and S2) using a Mini PROTEAN electrophoresis system (Bio-Rad, Madrid, Spain) at 4 °C after binding to a HIS-Select Nickel Affinity Gel (Merck Life Science S.L.U., Madrid, Spain), as previously described [5]. In detail, selected *E. coli* clones that expressed each protein, His-tagged at the C-terminus, were grown at 37 °C on solid LB agar medium (ThermoFisher Scientific, MA, USA; ref. 22700041) supplemented with 100 μg/ml Amp (ThermoFisher Scientific, MA, USA; ref. BP1760), and one colony was picked and used to inoculate 10 ml of LB broth plus antibiotic in a 0.25-l flask. The cultures were then incubated at 37 °C and 100 rpm overnight. Afterwards, 10 ml of this culture were used to inoculate 0.5-l of LB medium, which was then incubated to an $OD_{600\ nm}$ to approximately 0.7 (ranging from 0.55 to 0.75) at 37 °C. Protein expression was induced by adding IPTG (ThermoFisher Scientific, MA, USA; ref. 302790250) to a final concentration of approximately 1 mM, followed by incubation for 16 h at 16 °C. The cells were harvested by centrifugation at 5000 × *g* for 15 min to yield a pellet of 2–3 mg/ml pellet (wet weight). The wet cell pellet was frozen at −86 °C overnight, thawed, and resuspended in 15 ml of washing buffer (50 mM H_3PO_4 buffer pH 8.0, 0.3 M NaCl and 10 mM imidazole (Merck Life Science S.L.U., Madrid, Spain; ref. 56748)). Lysonase Bioprocessing reagent (Merck Life Science S.L.U., Madrid, Spain; ref. 71230) was added (4 μl/g wet cells), and incubated for 60 min on ice with rotating mixing. The cell suspension was sonicated using a pin Sonicator 3000 (Misonix, New Highway Farmingdale, NY, USA) for a total time of 5 min (10 W) on ice and centrifuged at 15000 × *g* for 15 min at 4 °C, and the supernatant was retained. The His-tagged proteins, native and engineered variants, were purified at 4 °C after binding to a HIS-Select Nickel Affinity Gel (Merck Life Science S.L.U., Madrid, Spain; ref. P6611), followed by ultrafiltration through low-adsorption hydrophilic 10000 nominal molecular weight limit cut-off membranes (regenerated cellulose, Merck Life Science S.L.U., Madrid, Spain; ref. UFC9010) to concentrate the protein solution. An extensive dialysis of protein solutions against 40 mM HEPES (Merck Life Science S.L.U., Madrid, Spain; ref. BP310-5) buffer (pH 7.0) was then performed using Pur-A-LyzerTM Maxi 1200 dialysis kit (Merck Life Science S.L.U., Madrid, Spain; ref. PURX60100), as follows. 5 ml of concentrated protein solution was dialyzed against 2-l buffer for 1 h at room temperature, after which the buffer was changed by another 2-l buffer and maintained for 1 h more. Then, the buffer was changed, and the dialysis was kept overnight at 4 °C. The dialyzed protein solution was recovered and concentrated as before. The concentrated protein solution (10 mg/ml) was then subjected to size-exclusion chromatography by a fast protein liquid chromatography (FPLC) equipment (LCC-500CI, Amersham Bioscience, Barcelona, Spain). The protein sample was loaded onto the FPLC coupled with a Superdex® 75 10/300 GL size exclusion column (Merck Life Science S.L.U., Madrid, Spain; ref. GE17-5174-01) pre-equilibrated with buffer HEPES buffer (pH 7.0). The proteins were eluted with the same buffer at a flow rate of 1 ml/min. Fractions with proteins were pooled, concentrated, and dialyzed against the HEPES buffer (pH 7.0), as before. Throughout the purification protocol, the fractions were analyzed by SDS–PAGE on 12% gels, in a Mini PROTEAN electrophoresis system (Bio–Rad, Madrid, Spain) [86], in which the proteins were stained with Seeband protein staining solution (Gene Bio-Application Ltd., Barcelona, Spain; ref. SB010). The protein concentration was determined according to Bradford (Bio-Rad protein assay dye reagent concentrate; Bio-Rad, Madrid, Spain; ref. 500-006) with bovine serum albumin as the standard [87]. In all cases, proteins were stored at -20 °C until use at a concentration of 10 mg/ml.

For quality control, 2 mutant genes were synthesized with non-productive active sites which were not reported to the group (CSIC) responsible for producing, purifying, and characterizing the enzymes. Once the assays were completed, the results of all variants, including those of the non-productive variants, were sent to the team in charge of the computational analysis and design of the mutations (BSC). After crosschecking, it was confirmed that none of the non-productive variants were active.

Expression of LCC-ICCG and HotPETase

The LCC-ICCG [25] gene inserted into a pET-21(+) expression vector with an Amp selection marker, with the following steps being the same as described above, and HotPETase gene [26] (see sequences in Data S1C) inserted into a pBbE8k expression vector with a kanamycin selection marker, were introduced into *E. coli* BL21 (DE3) (Agilent technologies, CA, USA; ref. 200131). *E. coli* clones that expressed each protein, His-tagged at the C-terminus, were grown at 37 °C on solid LB agar medium (ThermoFisher Scientific, MA, USA; ref. 22700041) supplemented with 30 μg/ml kanamicin (SERVA; ref. 26899), and one colony was picked and used to inoculate 10 ml of LB broth plus antibiotic in a 0.25-l flask. The cultures were then incubated at 37 °C and 100 rpm overnight. Afterwards, 10 ml of this culture were used to inoculate 0.5-l of LB medium, which was then incubated to an $OD_{600\ nm}$ to approximately 0.7 (ranging from 0.55 to 0.75) at 37 °C. Protein expression was induced by adding 10 mM L-arabinose (Merck Life Science S.L.U. (Madrid, Spain); ref. A3256-25G), followed by incubation for 16 h at 16 °C. The cells were harvested by centrifugation at 5000 × *g* for 15 min to yield a pellet of 2–3 mg/ml pellet (wet weight). Purification of both enzymes proceeded as described above.

Synthesis and expression of AldA and FucO

The amino acid sequences encoding AldA (propanediol oxidoreductase) and FucO (glycolaldehyde dehydrogenase) from *E. coli* MG1655 (GenBank accession numbers WP_000115943.1 and AAB40449.1) were used as a template for gene synthesis (Data S1C). The sequences of AldA and FucO were synthesized by GenScript Biotech (GenScript Biotech, EG Rijswijk, The Netherlands) and codon-optimized to maximize expression in *E. coli.* In brief, the genes were flanked by BamHI and HindIII (stop codon) restriction sites and inserted individually into a pET-45b(+) expression vector with an Amp selection marker (GenScript Biotech, Rijswijk, The Netherlands). This plasmid supports the expression of both N-terminal His6-fusion synthetic proteins, whose final amino acid sequences are MAHHHHHHVGTGSNDDDDKSPDPM-X (where X corresponds to the original sequences of the target enzymes). The plasmids containing each protein were subsequently introduced into *E. coli* BL21 (DE3) (ref. 200131; Agilent Technologies, CA, USA), and the soluble N-terminal His6-tagged proteins produced and purified at >98% purity, as detailed above. Expression of soluble proteins was confirmed in all cases, following the above protocol. Note: the *E. coli* BL21 (DE3) strain into which the pET-45b(+) plasmid containing *ald*A and *fuc*O was introduced, is herein referred to as *E. coli* BL21 (DE3) ($lsrB_{WT}$) – *fuc*O, *ald*A (S2).

ETE hydrolysis assays

The hydrolysis of ETE (ref. 465151, Merck Life Science S.L.U. (Madrid, Spain)), was assayed as previously described [6]. In brief: [ETE], 2 mM; [enzyme], 0.13 mg/ml; temperature, 37 °C; volume, 100 µl of HEPES buffer 20 mM, pH 7.0; agitation, 950 rpm; reaction time; up to 24 h. Reactions were carried out in sterile 2-ml safe-lock Eppendorf® polypropylene tubes (Eppendorf®, Hamburg, Germany; ref. 0030120094). After incubation, 900 µl of dimethyl sulfoxide (DMSO; Scharlau, Barcelona, Spain; ref. SV165) was added to stop the reaction, and the degradation products were immediately analyzed by HPLC. All experiments were carried out in biological replicates (n = 3), using as control samples without ETE, and enzyme.

Production of nPET

Nanosized nPET particles were obtained by pre-dissolving 0.1 g amorphous Goodfellow (GoodFellow Cambridge, Huntingdon, UK; ref. ES301445) for 2 h at 150 rpm and 25 °C in 10 ml 1,1,1,3,3,3,3-hexafluoro-2-propanol (Merck Life Science S.L.U., Madrid, Spain; ref. 105228-25G) and dispensed into a burette (Afora S.A., Barcelona, Spain; ref. A-6055). This solution is slowly (drop-by-drop) transferred (ca. 0.001 ml/min) into a 100 ml ice-cold water-containing beaker (in an ice bath), which was strongly agitated (250 rpm), to produce the precipitated nanosized PET polymer. The solvent (10 ml) was evaporated in a R-210 rotavapor (Buchi Ibérica S.L.U., Barcelona, Spain) with a hot water bath (60 °C). The vacuum was fixed at 137 mbar with an I-100 Interface. After solvent evaporation, the vacuum pressure was reduced to 72 mbar to eliminate part of the water to concentrate the nPET particle suspension to reduce the total volume to about one-third of its original value (approx. 40 ml final volume). The concentrated water solution containing nPET particles can be stored at 4 °C for approximately 2 months. The resulting pH values of the solutions were 7.0 ± 0.3. The concentration of particles in the obtained water solution was 4.0 ± 0.06 mg/ml, as measured by weighing the dry material from 1 ml solution in a Concentrator 5301 (Eppendorf®, Hamburg, Germany). The size diameter (n.d., 1–5.5 nm), crystallinity (%; 14.0%, 1.3%), cold crystallization energy (ΔH_c: 41.5 J/g, 32.8 J/g) and glass transition (T_G; 73.7 °C, 73.7 °C), melting (T_m: 245.9 °C, 246.7 °C), and cold crystallization (T_c: 199.6 °C, 200.6 °C) temperatures of fPET and nPET and, in the order they appear in parentheses, have been reported elsewhere [6].

In vitro assays for PET hydrolysis

Reaction conditions for nPET hydrolysis using purified enzymes were described previously [6]. In brief: [nPET], 1.65 mg/ml; [enzyme], 0.1 mg/ml; temperature, 37 °C; volume, 50 µl of HEPES buffer 20 mM, pH 7.0; agitation, 950 rpm; reaction time; up to 4 h. Reaction conditions for pPET hydrolysis were as follows: [pPET], 7 mg/ml; [enzyme], 0.1 mg/ml; temperature, 37-60 °C; volume, 50 µl of HEPES buffer 40 mM, pH 7.0; agitation, 950 rpm; reaction time, 0, 2, 4 and 24 h. All reactions were carried out in sterile 2-ml safe-lock Eppendorf® polypropylene tubes (ref. 0030120094). After incubation of all reactions, DMSO (Scharlau, Barcelona, Spain; ref. SV165) was added to stop the reaction, and the hydrolysis degradation products were immediately analyzed by HPLC. All experiments were carried out in biological replicates (n = 3), using as control samples without nPET, pPET, or enzyme. pPET was provided by Goodfellow Cambridge Ltd (Huntingdon, UK) (ref. ES30PD000132).

CRISPR/Cas9 genome editing and heterologous expression of *fuc*O & *ald*A

E. coli BL21 (DE3) ($lsrB_m$) – *fuc*O, *ald*A (S1) was prepared as follows. First, *E. coli* BL21 (DE3) ($lsrB_m$) was prepared and provided by GenScript Biotech (EG Rijswijk, The Netherlands). The methodology involved preparing host strain competent cells and transforming

them with the pCas plasmid. In brief, for gRNA plasmid construction and cleavage efficiency evaluation, 2-4 gRNAs were designed for each target locus. Genes were synthesized and sub-cloned into the pTargetF plasmid, followed by an evaluation of cleavage efficiency. The donor vector construction included synthesizing the donor template (dsDNA) with 5'&3' homologous arms of the insertion site. The donor template was then sub-cloned into the gRNA-expressing plasmid pTargetF. Electroporation and single clone screening involved transforming the gRNA-donor vector into the host strain containing the pCas plasmid. Colonies were spread on LB plates with kanamycin resistance (Kan^R) and streptomycin resistance (Sm^R), and up to 150 colonies were screened by PCR and validated through Sanger sequenci6ng. Finally, plasmids for genome editing were eliminated by inducing the positive strain with IPTG to eliminate the pTargetF plasmid. The strain was then cultured without pTargetF at 37 °C to eliminate the pCas plasmid. Then, an overnight culture of *E. coli* BL21 (DE3) *(lsr*B_m*)* was prepared in 10 ml LB media (Invitrogen, ThermoFisher, CA, USA; ref. 12780029) at 37 °C without shaking. Subsequently, a fraction corresponding to 1/10 of the LB volume was inoculated with the overnight culture and incubated at 37 °C with agitation at 220 rpm. $OD_{600\ nm}$ measurements were taken regularly until the culture reached an optimal density of 0.27-0.33. After achieving the desired $OD_{600\ nm}$ range, the culture was transferred to ice for 10 minutes. After that time, the culture was centrifuged for 10 minutes at 4 °C and 3000 *g*. The resulting supernatant was carefully discarded, and the sedimented cells were resuspended in 1/10 of the volume of the discarded supernatant using chilled $CaCl_2$ 50 mM, and directly used to introduce the pET-45b(+) expression plasmid containing *ald*A and *fuc*O (see above), to generate the strain *E. coli* BL21 (DE3) (*lsr*B_m) – *fuc*O, *ald*A. The CRISPR-Cas9 edited *E. coli* BL21 (DE3) (*lsrB*$_m$) strain (or strain S1) has been provided by GenScript Biotech (EG Rijswijk, The Netherlands) and is available upon request.

In vivo cultures in the presence of nPET

A single colony of each strain was inoculated into 2 ml of LB medium (Invitrogen, Thermo Fisher Scientific, MA, USA) supplemented with appropriated antibiotics in 15 ml Falcon tubes (ref. 62.554.502 Sarstedt AG & Co. KG, Nümbrecht, Germany). For S1 and S2 strains the antibiotic was 100 µg/ml Amp, and for $S1_{PCA}$ strain 25 mg/ml Cm and 100 mg/ml Amp.The cultures were allowed to grow overnight at 37 °C and 100 rpm in an orbital shaker (Thermo Scientific MaxQ 6000, Thermo Fisher Scientific, USA) until an $OD_{600\ nm}$ of approx. 1.0, and then centrifuged (800 *g* x 10 min, in an Eppendorf centrifuge 5810 R). Cells were washed three times with minimal medium M9 (Merck Life Science S.L.U., Madrid, Spain; ref. M6030) and resuspended in 1.5x M9 medium until an $OD_{600\ nm}$ of 1.0. A total of 1.5 ml of this cell suspension was added to 8.5 ml 1.5x M9 medium supplemented with 1.5x antibiotics, 1.5 mM IPTG, and 0.15 mg/ml glycerol (Merck Life Science S.L.U., Madrid, Spain; ref. 49767). To a 6.75 ml of this cell suspension a total of 3.25 ml of nPET particle suspension (concentration of particles of 4 mg/ml, prepared as detailed above) was added. Tests were performed in 50-ml Falcon tubes (Sarstedt, Nümbrecht, Germany; ref. 62.547.254). The tubes were incubated at 37 °C with 200 rpm agitation in a thermoshaker (Stuart orbital incubator SI500, Stuart Scientific Co. Ltd., Staffordshire, UK). During incubation, 100 µl of samples were taken at different times, and added to 900 µl of DMSO (from Scharlau, Barcelona, Spain; ref. SV165), so that the degradation products were immediately analyzed by HPLC. At the same times, 200 µl of samples were used to measure the $OD_{600\ nm}$ to evaluate cell's growth in a Synergy HT Multi-Mode Microplate Reader (with BioTek Gen5 2.0 software Agilent Technologies, Santa Clara, CA, USA). All experiments were carried out in biological triplicate (n = 3), using as control samples without nPET and cells.

Analysis of degradation products by HPLC

The samples were diluted with DMSO and filtered with 0.45 µm nylon filters (Membrane Solutions, Auburn, WA, USA; ref. SFNY025045N). The HPLC analysis was performed using a quaternary pump (Model 1100, Agilent Technologies, Las Rozas, Madrid, Spain) coupled to an autosampler (Model L2200, Hitachi, Chiyoda, Tokyo, Japan). The injection volume was 10 µl unless indicated. The column was a Zorbax Eclipse Plus C-18 (4.6 x 100 mm, 3.5 µm, Agilent Technologies, Las Rozas, Madrid, Spain; ref. 959961-902) at 40 °C and the mobile phase was a gradient of acetonitrile (ACN; from Scharlau, Barcelona, Spain; ref. AC0371) and water, both acidified with a 0.1 % (v/v) of formic acid (from Scharlau, Barcelona, Spain; ref. AC1080). The flow rate was 0.8 ml/min. The detection of peaks was carried out using a photodiode array detector (ProStar, Varian Inc., Palo Alto, California, USA), and integration was carried out using the Varian Star LC workstation 6.41 (Varian Inc., Palo Alto, California, USA) at a wavelength of 242 nm (for PET degradation products) and 260 nm (for PCA). The gradient is specified as follows: 0-3 min (10% ACN), 3 - 10 min (from 10 to 95% ACN), 10 - 14 min (95% ACN), 14 - 20 min (10% ACN, initial conditions). The total gradient time was 20 min. A calibration curve with pure degradation products (from 0 to 500 µM), purified by semi-preparative HPLC, was made to quantify the amount of degradation products. Semi-preparative HPLC for purifying the PET degradation products was performed using a quaternary pump (Model 600, Waters, Cerdanyola del Vallès, Barcelona, Spain) coupled to an autosampler (Varian ProStar,

Model 420, Varian Inc., Palo Alto, California, USA). The injection volume was 100 µl. The column was a Zorbax Eclipse XDB C-18 column (9.4 × 250 mm, 5 µm, Agilent Technologies, Las Rozas, Madrid, Spain; ref. 990967-202) at 40 °C. The column was coupled to a three-way flow splitter (Accurate, LC 14 Packings). The peaks were detected using a photodiode array detector (Varian ProStar, Varian Inc., Palo Alto, California, USA) at 242 nm. The mobile phase was ACN/H_2O in gradient, degassed with helium and acidified with 0.1% (v/v) formic acid. The flow rate was 6.0 ml/min. The gradient (total: 15 min) was as follows: 2 min, 10% ACN; 5 min, 10% to 95% ACN; 1 min, 95% ACN and 7 min 10% ACN. The solvents were evaporated in an R-210 rotary evaporator (Buchi Ibérica S.L.U., Barcelona, Spain).

Analysis of degradation products by mass spectrometry (ESI/MS)

Samples were diluted with methanol (instead of DMSO, as detailed above) and were analyzed by Reverse Phase High-Performance Liquid Chromatography-Mass Spectrometry (RP-HPLC-MS) in a Waters Alliance e2695 Separations Module coupled to a Waters 2998 Photodiode Array Detector and coupled to a single quadrupole Waters Acquity QDa mass spectrometer (Waters Cromatografía, SA; Barcelona, Spain). Compounds were analyzed by reverse phase chromatography using a 2.1 mm × 5 mm Waters Sunfire C18 RP precolumn (Waters Cromatografía, SA; Barcelona, Spain; ref. 186002539) and 2.1 mm × 100 mm Waters Atlantis T3 C18 RP column (Waters Cromatografía, SA; Barcelona, Spain; ref. 186003718), operating at 0.35 ml/min. The injection volume of the sample was 6 µl. Compounds were eluted using a 10 min gradient from 15 to 95% solvent A-B (solvent A: acetonitrile, solvent B: water), which includes a 5% fixed percentage of solvent C (solvent C: 2% formic acid in water), being the concentration of formic acid in all the gradient a 0.1%. After the separation, the sample was analyzed by optical detection from 190-700 nm with a resolution of 1.2 nm Waters 2998 PDA Detector) and by mass analyzer (Waters Acquity QDa Detector) using an Electrospray (ES) Interface in Positive and Negative Mode with a Capillary Voltage of 0.8kV and a Cone Voltages of 20V y 40V, being the Probe Temperature of 600 °C and the Source Temperature of 120 °C. Compounds were detected in Full Scan MS from 85 to 1250 m/z, with automated mass resolution control of 0.7 Da. The main products of each sample ionized at m/z 357 ($C_{18}H_{14}O_8$) and m/z 401 ($C_{20}H_{18}O_9$). These findings are consistent with these products being TET and TETE. All other original data is provided by the Unidad de Análisis Instrumental from the Instituto de Química Médica (IQM-CSIC), Spain; raw data can be provided upon request by the LC-MS Unit.

Analysis of nPET by AFM and SEM

Gold-coated nPET was prepared by a method adapted from Dawson and colleagues 2000 [88] and 2001 [89]. Briefly, 20 ml of a 1 mg/ml suspension of nPET particles was prepared in 40 mM HEPES buffer at pH 7.0. Separately, a 10 mM HAuCl solution was prepared by dissolving 0.0985 g of HAuCl (Merck Life Science S.L.U., Madrid, Spain; Ref. 520918) in 25 ml of ultrapure water, and a 10 mM NaBH solution was freshly prepared by dissolving 9.46 mg of NaBH (Merck Life Science S.L.U., Madrid, Spain; Ref. 452882) in 25 ml of ultrapure water. Then, 20 ml of the 10 mM HAuCl solution was added dropwise to the nPET suspension under vigorous stirring at room temperature. Immediately afterward, 20 ml of the 10 mM NaBH solution was added dropwise under continued vigorous stirring for 30 seconds. Freshly prepared gold particles were directly used for AFM and SEM. For AFM, a suspension of gold-coated nPET particles (1 mg/ml) was prepared and placed onto a silicon wafer substrate (agar scientific, UK, G3390). The sample was dried at 25 °C for 2 hours under atmospheric conditions. AFM micrographs were acquired using a Bruker (USA) MultiMode® scanning probe microscope in tapping mode with an antimony-doped Si rectangular cantilever (Bruker, RTESPA-150; tip radius = 8 nm, f = 150 kHz, k = 5 N/m). The image processing (flattening and height adjustment) and analysis (roughness and line profiles) of the micrographs were performed using the WSxM free software package and are presented unfiltered. Height distributions were examined on the entire micrograph. For SEM, a suspension of gold-coated nPET particles was prepared and spread on a silicon substrate. The sample was allowed to dry at room temperature under atmospheric conditions and subsequently sputter-coated using a Quorum Technologies SC7620 (UK) system with gold for 10 seconds at 20 mA. Secondary electron micrographs were acquired using a Zeiss (Germany) SUPRA® 40VP scanning electron microscope using the InLens mode with an accelerating voltage of 5 kV at different magnifications, ranging from 5,000 to 200,000 X. Particle diameters were measured on the SEM micrographs using the ImageJ free software package (at least 100 measurements were performed for each sample).

Growth and fitness analysis

For the growth assays, stock solutions of E (Merck Life Science S.L.U., Madrid, Spain; ref. 324558) and glucose (Merck Life Science S.L.U., Madrid, Spain; ref. G5767) were prepared at 500 mg/ml in M9, and glycerol (Panreac Química SAU, Barcelona, Spain; ref. 122329) at 10 mg/ml in M9. These solutions were sterilized by filtration through a 0.2-µm polyethersulfone filter (VWR International,

Barcelona, Spain; ref. 28145-501). One colony of strains S1 and S2 was picked from a glycerol stock (prepared from an overnight culture at 37 °C, to which glycerol was added to a final concentration of 20% v/v) and used to inoculate 10 ml of LB broth supplemented with 100 µg/ml Amp, in a 0.25-l flask. The cultures were then incubated at 37 °C and 1000 rpm overnight in an orbital shaker (Thermo Scientific MaxQ 6000, Thermo Fisher Scientific, USA). Afterwards, the cultures were centrifuged in an Eppendorf centrifuge 5810 R (Eppendorf®, Hamburg, Germany) at 5000 g for 15 minutes to obtain a pellet, which was washed three times with M9 medium. Dilutions were then prepared to an optical density (OD) at 600 nm ($OD_{600\ nm}$) of 1.0 in either LB or M9 medium, measured in a BioPhotometer (No. 6131 25728, Eppendorf AG, Hamburg, Germany). For the LB cultivation tests, 180 µl of LB medium supplemented with 1 mM IPTG and 100 µg/ml Amp, and 20 µl of the cell stock at an $OD_{600\ nm}$ of 1.0 were added to each well, resulting in a final cell $OD_{600\ nm}$ of 0.1. For the M9 cultivation tests with glucose, 176 µl of M9 supplemented with 1 mM IPTG and 100 µg/ml Amp, 4 µl of glucose stock solution, and 20 µl of the cell stock at an $OD_{600\ nm}$ of 1.0 were added, resulting in a final glucose concentration of 10 mg/ml and a final cell $OD_{600\ nm}$ of 0.1. For the M9 medium cultivation tests with E, 174 µl of M9 supplemented with 1 mM IPTG and 100 µg/ml Amp, 4 µl of E stock solution (500 mg/ml), 2 µl of glycerol stock solution (10 mg/ml), and 20 µl of the cell stock at an $OD_{600\ nm}$ of 1.0 were added, resulting in final concentrations of 10 mg/ml of E and 0.10 mg/ml of glycerol, and a final cell $OD_{600\ nm}$ of 0.1. For the M9 medium assays with glycerol, 178 µl of M9 supplemented with 1 mM IPTG and 100 µg/ml Amp, 2 µl of glycerol stock solution (10 mg/ml), and 20 µl of the cell stock at an $OD_{600\ nm}$ of 1.0 were added, resulting in a final glycerol concentration of 0.10 mg/ml and a final $OD_{600\ nm}$ of 0.1. Control cultures without cells were included in all cases. The final volume in each well was 200 µl. The cultures, performed in triplicate, were maintained in a sterile 96-well U-bottom microplate (Greiner Bio-One International GmbH, Kremsmünster, Austria; ref. 650161), and the $OD_{600\ nm}$ was recorded every 10 minutes for 24 hours using a BioTek Synergy H1 Multimode Reader (Agilent, CA, USA) with constant shaking at 807 rpm.

Selection coefficients (S) were calculated using Equation 4. In all cases, the maximum growth rate (µmax) was defined as the highest growth rate during the exponential phase. The standard error was calculated from the standard deviation of growth rates in the linear region of the growth curve across triplicate measurements.

$$S = 1 - \frac{\boldsymbol{\mu} native}{\boldsymbol{\mu} edited} \quad [4]$$

Equation 4**.** Equation for calculating fitness (S) based on the ratio of growth rates between the engineered/edited strain (S1) and the reference/native strain (S2).

In vivo degradation of nPET by native bacterial strains

S. stutzeri was inoculated in 5 ml of LB broth, while *H. litoralis, H. oceani, H. aestusnigri, and H. bauzanensis* were inoculated in 5 ml of LB broth supplemented with 3% NaCl. These strains produce PETase like enzymes as indicated by halo formation on agar plates containing Impranil® DLN-SD emulsion (Covestro, Leverkusen, Germany) [35]. Cultures were grown at 28 °C and 150 rpm overnight. After incubation, the cultures were centrifuged, and the cells were washed three times with 1x M9 minimal medium. The cells were then resuspended in 1x M9 medium to achieve a final $OD_{600\ nm}$ of 1. A stock solution of 1.5x M9 medium and a stock of 10 mg/ml glycerol were prepared. For the reaction, a mixture was prepared with a final volume of 500 µl containing 1x M9 medium, PET nanoparticles at a final concentration of 1.3 mg/ml, 0.1 mg/ml glycerol, and cells at an $OD_{600\ nm}$ of 0.1. Reactions were carried out at 28 °C and 950 rpm for 24 hours. All experiments were performed in triplicate. Samples were prepared in 2 ml clear 9-425 screw top vials (Membrane Solutions, Auburn, WA, USA; ref. LBSV022C) equipped with 0.25 ml micro-inserts, 31 × 6 mm, conical, clear glass, 15 mm top (Membrane Solutions, Auburn, WA, USA; ref. LBSV222CSS), and sealed with pre-slit blue PTFE/white silicone septa and blue screw caps with hole for 2 ml vials (Membrane Solutions, Auburn, WA, USA; ref. LBSV222CSS), by adding 50 µl of the reaction mixture to 200 µl of acetonitrile containing 1% trifluoroacetic acid (TFA). The samples were centrifuged at 10,000 rpm for 3 minutes, and 200 µl of the supernatant was transferred to 600 µl of Milli-Q H_2O. Samples were analyzed via RP-UHPLC using the method described previously [90].

Cloning of the *tph*A2A3BA1 gene cluster from *C. thiooxidans* S23 for T catabolism

The *tph*A2A3BA1 gene cluster from *C. thiooxidans* S23, which is responsible for T catabolism, was cloned into the pBBR1MCS vector with Cm resistance (Cm^R), yielding the pBBR1MCS::*tph*A2A3BA1 construct [91,92]. The construct was then electroporated into

the *E. coli* strains S1 and S2 following the standard EMBL protocol involving washing cell pellets with 10 % glycerol and GenePulser Xcell™ (BioRad, Feldkirchen, Germany; ref. 1652667) and the settings provided by the manufacturer for *E. coli* cells (1 mm cuvette, 1.8 kV, 25 μF, 200 Ω). Transformants were selected on plates containing 25 mg/ml Cm and 100 μg/ml Amp, respectively, and the presence of the plasmid(s) was confirmed by PCR.

Verification of T-to-PCA conversion in engineered *E. coli* strain

E. coli $S1_{PCA}$ strain was grown at 37 °C on solid LB agar medium (ThermoFisher Scientific, MA, USA; ref. 22700041) supplemented with 25 mg/ml Cm and 100 μg/ml Amp. One colony was picked and used to inoculate 10 ml of LB broth with antibiotics in a 0.25-l flask. The cultures were then incubated at 37 °C and 100 rpm overnight. To verify the T conversion to PCA in engineered *E. coli* strains 1 ml of this culture was used to inoculate 50 ml of LB medium with antibiotics, which was incubated at 37 °C until the $OD_{600\ nm}$ reached approximately 0.7 (ranging from 0.55 to 0.75). Protein expression and conversion was induced by adding IPTG (ThermoFisher Scientific, MA, USA; ref. 302790250) to a final concentration of approximately 1 mM, and by adding T at a final concentration of 10 mM (using a stock solution of 1 M in DMSO), followed by incubation at 37 °C. During incubation, 100 μl samples (in triplicates) were taken at different time points and added to 900 μl of DMSO (Scharlau, Barcelona, Spain; ref. SV165), to immediately analyze the remaining amount of T and the formation of the metabolic product PCA by HPLC as detailed above.

QUANTIFICATION AND STATISTICAL ANALYSIS

Standard deviations were calculated via the STDEV. S function in Excel 2019. Statistical analyses were performed using the GraphPad Prism 10.0. All experiments were performed with three replicates, and the error bars in the figure legends and tables represent the means ± standard deviations.